• U C • FCTUC FACULDADE DE CIÊNCIAS E TECNOLOGIA
UNIVERSIDADE DE COIMBRA

DEPARTAMENTO DE ENGENHARIA MECÂNICA

Influence and stability of deep rolling residual stresses in the steel AISI 1045 subjected to multi-level loads

Dissertação apresentada para a obtenção do grau de Mestre em Engenharia Mecânica na Especialidade de Produção e Projecto

Autor

Francisco João Duarte de Araújo

Orientadores

Dr.-Ing. Ulf Noster

Professor Doutor João Paulo da Silva Gil Nobre

Júri

Presidente	**Professora Doutora Cristina Maria Gonçalves dos Santos Louro** **Professora Auxiliar da Universidade de Coimbra**
Vogais	**Professor Doutor João Paulo da Silva Gil Nobre** **Professor Auxiliar da Universidade de Coimbra**
	Professor Doutor José Domingos Moreira da Costa **Professor Associado com Agregação da Universidade de Coimbra**
	Professor Doutor António Adriano Castanhola Batista **Professor Auxiliar da Universidade de Coimbra**

Em cooperação com a Universidade de Kassel

Institut für Werkstofftechnik – Metallische Werkstoffe Universität Kassel

Coimbra, Setembro, 2013

Aos meus pais.

Acknowledgements

This paper is a result of six months of work that allows me to finish the Master in Mechanical Engineering. As this work was realized out of my home country, I must to acknowledge some people that made part of this work.

First of all, I am deeply thankful to my parents for making this work possible. Despite my personal effort, this work wouldn´t be done without their guidance, encouragement and all the support.

Special acknowledgement has to be given to my friends in Kassel. They were part of my life in the last six months and partners of adventures, good and bad moments. Their contribution to this work was very important in terms of encouragement and companionship. Thanks to Miika Saavalainen, Fala Buggy, Brianna McCain, Hana Holcová, Ilona Féki, and especially, to Karolína Zelená. Also, besides the distance, my friends in Portugal were always in my thoughts.

I am very grateful to Dr.-Ing. Ulf Noster for his supervision and contribution in this work. Special thanks to Prof. Dr. João Paulo Nobre for his assistance and corrections. I am also thankful to Dr.-Ing. habil. Berthold Scholtes for giving me the opportunity to do this work in Institute of Materials Science - Metallic Materials of University of Kassel. I have also had great benefit from the technical assistance from Dr.-Ing. Rolf Diederich, Stephen Krella, Christian Franz, Dipl.-Wirtsch.-Ing. Kerstin Anten, and the people from IfW that somehow contributed for this work.

Resumo

O objectivo deste trabalho é estudar a influência e estabilidade de tensões residuais no comportamento à fadiga no aço AISI 1045. O processo de laminagem profunda foi usado como tratamento mecânico para introduzir no material um estado de tensões residuais compressivas em zonas próximas da superfície. Testes à fadiga uniaxiais foram realizados de modo a avaliar o comportamento à fadiga do material tratado mecanicamente. Foram definidas três amplitudes de 300, 350 e 400 MPa aplicadas em ciclos de tensão constante e combinadas em ciclos de tensão variável. As tensões residuais e a largura do pico de difracção foram calculadas através de difracção de raio-X. O polimento electrolítico foi usado como processo para remover camadas de material. Medições de dureza foram realizadas de forma a fazer uma ligação entre o endurecimento causado pela laminagem profunda e o comportamento à fadiga.

Os resultados mostram que o comportamento do material sujeito à fadiga é influenciado pela tensão aplicada. Elevadas amplitudes de tensão provocam elevadas deformações plásticas e menor resistência à fadiga. É observada uma melhoria do comportamento à fadiga do material tratado mecanicamente em relação ao não tratado. O material sujeito à fadiga exibe uma relaxação de tensões residuais que é mais pronunciada para amplitudes de tensão mais altas. Em fadiga de tensão variável, a deformação plástica aumenta ou diminui quando se varia a tensão aplicada. O número de ciclos aplicados em cada bloco de tensão influencia a estabilidade das tensões residuais induzidas. A relaxação das tensões residuais é bastante influenciada para ciclos de tensão constante seguidos de apenas meio ciclo com uma tensão mais alta ou mais baixa do que a tensão anterior.

Palavras-chave: Laminagem Profunda, Fadiga, Tensões Residuais, Encruamento, Aço AISI 1045, Ciclos de tensão variável.

Abstract

The main objective of the work presented is the study of the influence and stability of near surface zone of deep rolled steel AISI 1045 subjected to cyclic loading. Deep rolling process was applied as a mechanical surface treatment to induce a compressive residual stress state in near surface zones of material. Tension/Compression fatigue tests were performed in order to evaluate cyclic deformation behaviour after the mechanical surface treatment. Three stress amplitudes of 300, 350 and 400 MPa were used in constant amplitude loading and combined in variable amplitude loading. Residual stress and FWHM (full width at half maximum) distribution measurement were carried out by X-ray diffraction regarding the influence of cyclic loading on near surface zone properties stability. Electropolishing was utilized as a removal material process. Microhardness measurements were carried out concerning determination of work hardened surface layers.

Results show that cyclic deformation behaviour is influenced by stress amplitude. High stress amplitudes lead to high strain amplitudes and low fatigue lifetimes. An improvement of lifetime is achieved for deep rolled specimen showing the influence of mechanical surface treatment on fatigue lifetime. Residual stress distribution exhibits a relaxation due to cyclic loading, which is higher for higher stress amplitudes. In variable amplitude loading, a change of stress amplitude leads to an increase or decrease of plastic strain amplitude for higher or lower stress amplitudes, respectively. The number of cycles of each load block influences stability of residual stress state. A load block in constant amplitude loading followed by only half of one cycle of higher or lower stress amplitude than the previous block influences significantly residual stress relaxation.

Keywords Deep rolling, Fatigue, Residual stresses, Work hardening, Steel AISI 1045, Variable amplitude loading.

INDEX OF CONTENTS

INDEX OF FIGURES

INDEX OF TABLES

SYMBOLS

{hkl} – lattice plane

$\Delta\varepsilon$ – Total strain

$\Delta_{\varepsilon_e}/2$ – Elastic strain amplitude

$\Delta_{\varepsilon_p}/2$ – Plastic strain amplitude

$\Delta\sigma$ – Total stress

ΔK – Stress intensity factor range

δ – Kronecker´s symbol

ε – Strain

ε'_f – Fatigue strength coefficient

Θ – Angle between the incident beam and the diffracted planes

λ – Wavelength

σ - Stress

σ_a – Stress amplitude

σ_e – Stress amplitude under mean stress

σ'_f – Fatigue strength coefficient

σ_m – Mean stress

σ_u – Tensile strength

σ_y – Yield strength

υ – Poisson´s ratio

ψ – Angle of the specimen

a – Crack length

A – Amplitude ratio

d – Distance between lattice planes

d_0 - Distance between lattice planes in free-stress state

E – Young modulus

I - Intensity

K – Stress intensity factor

K^{eff} – Effective stress intensity factor

K_{res} – Stress intensity factor due to presence of residual stresses

N – Number of cycles

N_f – Number of cycles to failure

R – Stress ratio

$S_1\{hkl\}$ – Elastic constant used in X-ray diffraction

$1/2S_2\{hkl\}$ - Elastic constant used in X-ray diffraction

1. INTRODUCTION

Field of residual stresses in materials has become one of the most important aspects in engineering design once they are present in all mechanical and structural components. Since the first European Conference on Residual Stresses (ECRS) in Karlsruhe (Germany, 1983), lot of papers and investigations with residual stresses as a main topic came out in many others ECRS and in the International Conferences on Residual Stresses (ICRS). Nowadays, the two cycles of conferences are alternating every two years with the next ECRS taking place in Troyes in 2014 (9th European Conference on Residual Stresses, 2013).

In these conferences topics such as origin, measurement, prediction, modeling, and effects of residual stresses have been presented and discussed. Residual stresses arise in materials as a result of manufacturing processes, heat and mechanical treatments. Origin of residual stresses in manufacturing processes are due to inhomogeneous plastic deformations and thermal loading that can cause significant temperature differences between near surface regions and core layers, as well as, phase transformations (Kloos and Kaiser, 1991). Also, welding is a well-studied process that causes residual stresses due to shrinkage processes, quenching processes and phase transformations (Zinn and Scholtes, 2002). Measurement of residual stresses distributions can be made by the classic and destructive hole-drilling method (Nobre et al., 2000) or by the well-known and non-destructive X-ray diffraction method (François et al., 1996). Neutron diffraction (Hutchings and Krawitz, 1992) is also a very used method in residual stress measurement.

For engineering design, compressive residual stresses induced by mechanical surface treatments assume a particular importance since they are desirable and beneficial for fatigue lifetime. Mechanical surface treatments such as shot peening, deep rolling and laser shock peening create a compressive residual stress field in near surface regions of the material. Work hardening and microstructure changes are also produced by these mechanical surface treatments. As a consequence, an improvement of fatigue lifetime can be obtained since compressive residual stresses and work hardening have effect on fatigue crack initiation and fatigue crack propagation (Glinka, 1987). Also, a lower surface

roughness produced by deep rolling process causes an enhancement on fatigue lifetime since it eliminates many stress concentration points at the surface (Altenberger, 2005b).

The lifetime enhancement depends on the material, the parameters of the mechanical surface treatment used, the kind of cyclic load, and the stability of the residual stress state and strain hardening. The influence of these parameters on fatigue behaviour has been widely studied for a lot of materials and mechanical surface treatments. For the shot peened steel AISI 1045, Martin et al. (1998), found an improvement of cyclic deformation behavior for higher Almen intensities. Also, in deep rolled steel AISI 1045, a higher deep rolling pressure leads to longer fatigue lifetimes as observed by Altenberger (2000).

Yet, service loads are mostly multi-level and most of the works in this field are for constant amplitude loading. It is known that fatigue behaviour under variable amplitude loading can be described by the fatigue crack growth rate, but no works were found regarding the effect of residual stresses on that. Then, study of the stability of mechanically surface zone under variable amplitude loading is very interesting.

In this work, influence and stability of near surface zone at multi-level load of deep rolled AISI 1045 is studied. Fatigue tests under constant and variable amplitude loading were performed, residual stress and FWHM (full width at half maximum) distributions were measured in order to link their stability to cyclic deformation behaviour. Microhardness measurements were carried out to evaluate strain hardening produced by deep rolling.

Hence, literature review regarding fatigue behaviour and residual stresses was made. In chapter 2, the way residual stresses arise and a brief presentation of deep rolling process as a inducer of residual stresses is written. A theoretical analysis of X-ray diffraction method is also presented. In the end, effects of residual stresses in cyclic deformation behaviour are reviewed. Chapter 3 includes all methodology and parameters concerning to deep rolling, fatigue tests, X-ray diffraction and hardness measurements. Results with residual stresses and FWHM distribution, microhardness depth profiles, and cyclic deformation curves are presented in chapter 4. A discussion of results linked to literature review is made in chapter 5. Finally, chapter 6 presents the main conclusions of this work.

2. LITERATURE REVIEW

2.1. Fatigue and Fracture Mechanics

The way the mechanical components fail is most of the times by fatigue. The definition of fatigue by ASTM (American Society for Testing and Materials) is: "*The process of progress localized permanent structural changes occurred in a material subjected to conditions that produces fluctuating stresses at some point or points and that may culminate in cracks or complete fracture after a sufficient number of fluctuations*". In other words this means that when a material is subjected to variable loading which causes cyclic variations in the applied stress or strain, cracks can appear and lead to failure. This failure is called by fatigue failure.

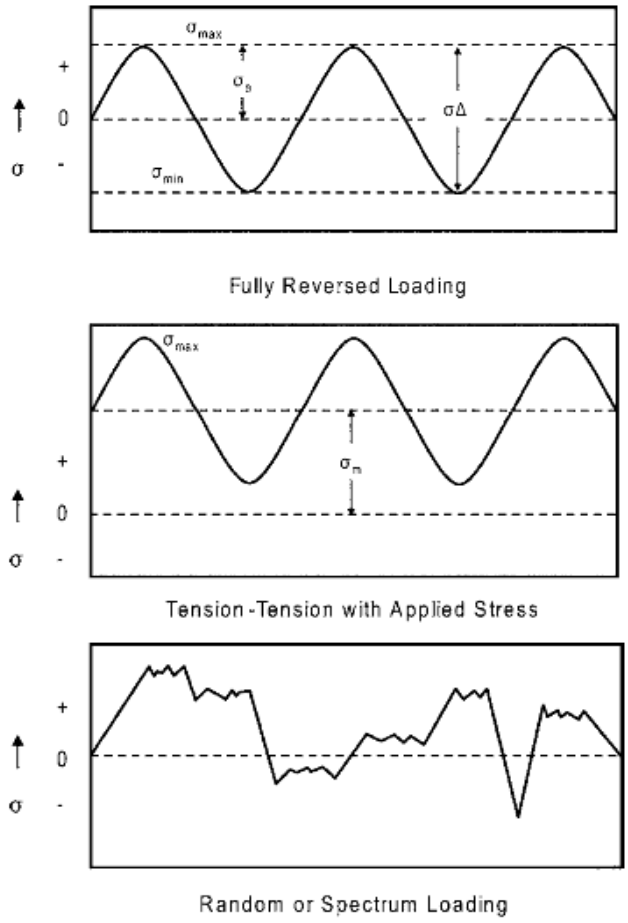

Figure 1 - Typical loading cycles (Campbell, 2008).

The fatigue failure can be divided in four stages (Branco, 1998):

1. Crack Nucleation;
2. Microscopic Crack Growth;
3. Crack Propagation;
4. Fracture.

These stages are the macro mechanisms of fatigue failure and the first and the second stage together are the stage of crack initiation. The crack initiation stage consists in a crack nucleation that has origin in points of stress concentrations like fillets, notches, tool marks or in microstructure defects. At the point where the crack nucleates, as a stress concentration point, the induced stress increase above the material yield strength and cyclic plastic strain occurs. As a result of plastic deformation occurred, dislocation movements arise creating a crack. The crack propagates as a result of stress level increase and then the cross sectional area gets insufficient to resist the applied stress resulting in fracture. Figure 2 shows how a crack propagates step by step in cylindrical specimen.

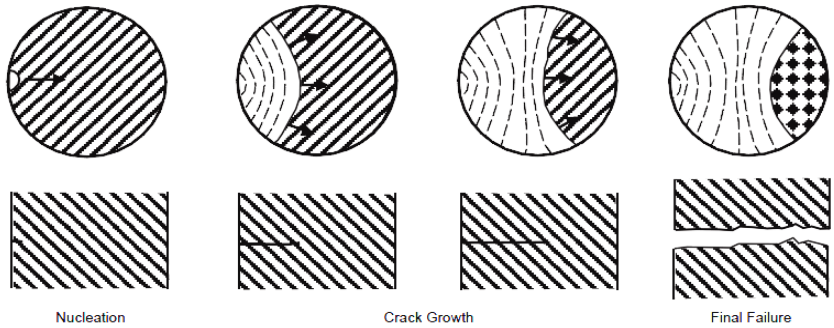

Figure 2 - Typical propagation of a crack (Campbell, 2008).

However, all the materials resist in a different way to this mechanisms that leads to fatigue failure. The fatigue behavior is function of many different parameters such as (Branco, 1998):

- Surface texture, coatings and residual stresses at the component surface;
- Size and geometry of the component;
- Stress concentrations zones;
- Stress state;
- Environment conditions;
- Temperature;
- Material and heat treatment.

The contribution of these parameters to fatigue behavior is well known and they are not specified here, however, it is detailed in Branco (1998). Further this parameters, the type of loading also has effect on fatigue behavior, namely, the mean stresses. Figure 1 shows typical loading cycles for constant amplitude stressing. For the fully reversed loading the mean stress is zero, whilst the second type has a nonzero mean stress. The influence of mean stress is shown in figure 3. It is noted that the increase of mean stress cause a reduction in the fatigue life. From the figure it can be said that the stress range is the difference between the maximum and the minimum values of stress. Thus, half the range which is called by stress amplitude or alternating stress is defined in (2.1). The mean stress is the average of the maximum and minimum values defined in (2.2).

$$\sigma_a = \frac{\sigma_{máx} - \sigma_{min}}{2}. \tag{2.1}$$

$$\sigma_m = \frac{\sigma_{máx} + \sigma_{min}}{2}. \tag{2.2}$$

Other useful mathematical expressions are the stress ratio given by (2.3) and amplitude ratio in (2.4):

$$R = \frac{\sigma_{min}}{\sigma_{máx}}. \tag{2.3}$$

$$A = \frac{\sigma_a}{\sigma_m}. \tag{2.4}$$

Thus, the stress ratio is $R = -1$ for fully reverse loading, $R = 0$ for zero-tension fatigue, and $R = 1$ for a static load.

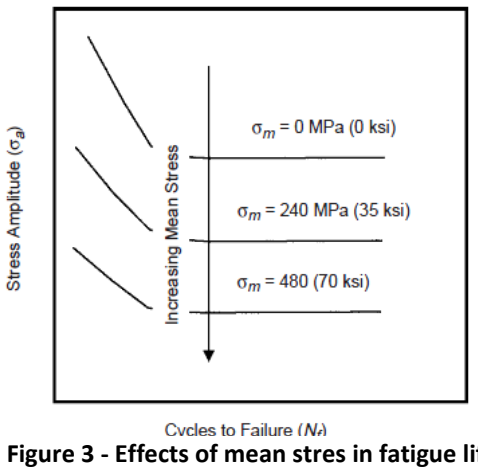

Figure 3 - Effects of mean stres in fatigue life represented by S-N curves (Campbell, 2008).

As represented in figure 3 fatigue lifetime can be plotted with stress amplitude-life curves. These curves are known as S-N curves and are obtained from fatigue tests data for constant amplitude loading. Also, mean stress effects on fatigue life can be represented in constant-life diagrams, as shown in figure 4. Three curves are plotted representing the most well-known models for the fatigue life plots, Soderberg, Goodman and Gerber. The mathematical expressions for these models are given by (Campbell, 2008):

$$\sigma_a = \sigma_e \left[1 - \left(\frac{\sigma_m}{\sigma_u}\right)\right], \tag{2.5}$$

$$\sigma_a = \sigma_e \left[1 - \left(\frac{\sigma_m}{\sigma_y}\right)\right], \tag{2.6}$$

$$\sigma_a = \sigma_e \left[1 - \left(\frac{\sigma_m}{\sigma_u}\right)^2\right], \tag{2.7}$$

where σ_a is the stress amplitude, σ_e is the stress amplitude under zero mean stress, σ_y and σ_u are parameters from material, the yield and tensile strength, respectively.

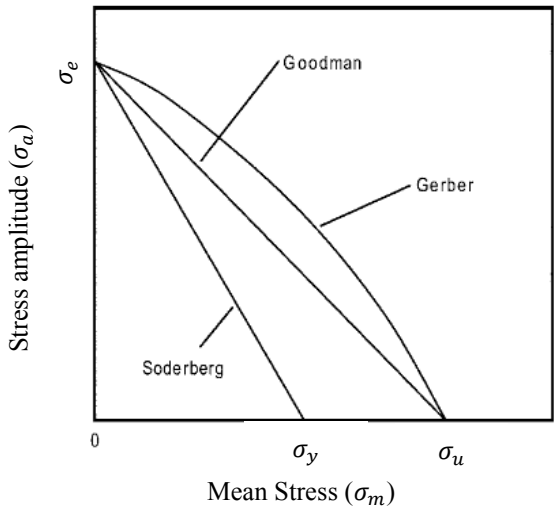

Figure 4 - Constant-life diagrams comparing the models of Soderberg, Goodman and Gerber (Campbell, 2008).

However, in reality, mechanical components are most of the time subjected to variable amplitude loading with different stress amplitudes, mean stresses and loading frequencies. Thus, the fatigue life is predicted in a different way including the cumulative

damage induced by various blocks of different stress amplitudes. A simple criterion to predict the fatigue life with this type of fatigue loading is the Palmgren-Miner rule employed by A. Palmgren in Sweden in 1920s. M. A. Miner gives the name because he has wrote the rule on paper in 1945 and since then this rule became known. The rule is widely known as Miner´s rule and is expressed in (2.8).

$$\frac{N_1}{N_{f1}} + \frac{N_2}{N_{f2}} + \frac{N_3}{N_{f3}} + \cdots = \sum \frac{N_j}{N_{fj}} = 1, \tag{2.8}$$

where N_1 is the number of cycles for an applied stress σ_{a1}, and N_{f1} is the number of cycles to failure from the S-N curve. The fatigue failure is expected when the sum of the life fractions for each stress amplitude applied equals the unity.

This rule states implicitly that (Suresh, 1998):

- The number of stress cycles imposed on a component, expressed as a percentage of the total number of stress cycles of the same amplitude necessary to cause failure, gives the fraction of damage;
- The order in which the stress blocks of different amplitudes are imposed does not affect the fatigue life;
- Failure occurs when the linear sum of the damage from each load level reaches a critical value.

In figures 5 and 6 is shown the use of the Palmgren-Miner rule for fully reversed loadings and for a variable loading with different mean stresses. However, cumulative damage and failure under variable amplitude loading conditions are influenced by many mechanisms (Suresh, 1998). Hence, Miner´s linear damage rule can predict fatigue life incorrectly for some cases.

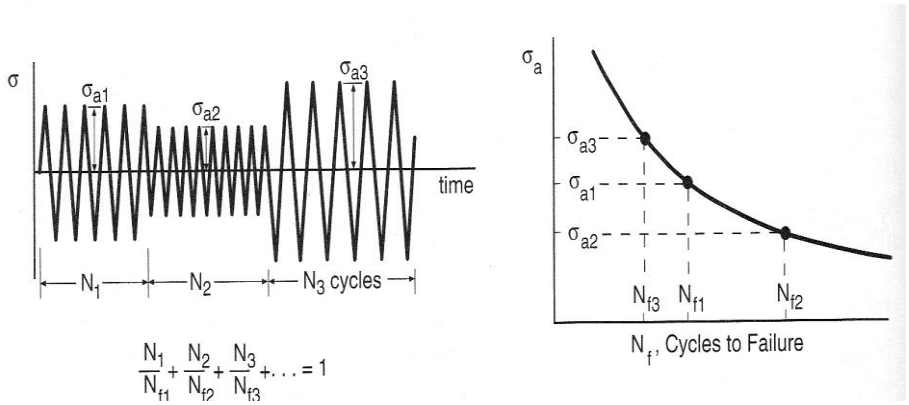

Figure 5 - Life prediction using Miner´s rule for variable amplitude loading which is fully reversed (Dowling, 2013).

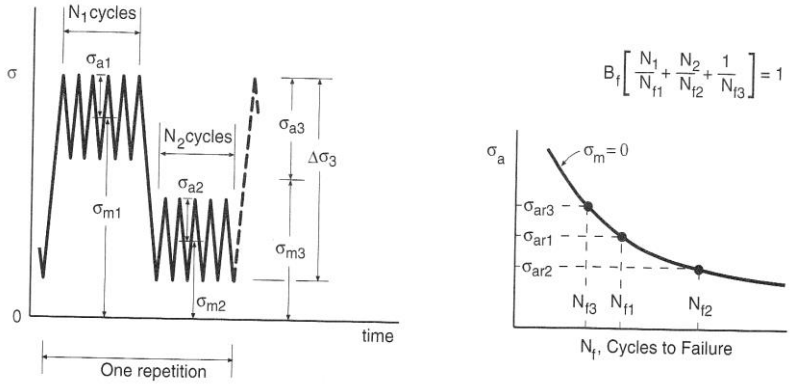

Figure 6 - Life prediction using the Miner´s rule for variable amplitude loading with mean level shifts (Dowling, 2013).

High-Cycle fatigue occurs for a large number of cycles, usually, more than 10^5 cycles. Low-Cycle fatigue involves a number of cycles smaller than 10^5 cycles, but with an applied stress that induces plastic strains. The response for this type of cyclic loading is a hysteresis loop as represented in figure 7. Starting from point O to A the material is in tension reaching the maximum tensile applied stress and the maximum strain in A. From A to D the material is on unloading and in D the applied stress is zero. The response to compressive applied stress is represented by the curve from point D to B. From B the material is unloaded and tensile stress is applied following the curve until A as shown. The area of hysteresis loop represents the work done or the energy loss per cycle. The total strain $\Delta\varepsilon$ is the sum of the elastic $\Delta\varepsilon_e$ and plastic $\Delta\varepsilon_p$ components:

$$\Delta\varepsilon = \Delta\varepsilon_e + \Delta\varepsilon_p. \tag{2.9}$$

The High-Cycle fatigue is described by the Basquin equation in (2.10) where the nominal strains are elastic.

$$\sigma_a = \frac{\Delta\varepsilon_e}{2} E = \sigma'_f (2N)^b, \tag{2.10}$$

where σ_a is the stress amplitude, $\Delta\varepsilon_e/2$ is the elastic strain amplitude, E is the Young modulus of the material, σ'_f is the fatigue strenght coefficient, 2N is the number of reversals to failure, and b is the fatigue strength exponent. The Coffin-Manson relation describes the Low-Cycle fatigue as function of plastic strain amplitude expressed in (2.11).

$$\frac{\Delta\varepsilon_p}{2} = \varepsilon'_f (2N)^c, \tag{2.11}$$

where $\Delta\varepsilon_p/2$ is the plastic strain amplitude, ε'_f is the fatigue ductility coefficient, 2N is the number of reversals, and c is the fatigue ductility exponent.

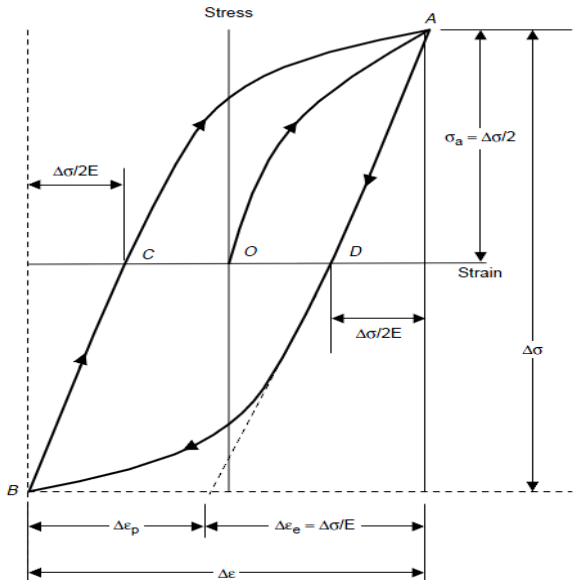

Figure 7 - Stress-Strain hysteresis loop for cyclic loading (Campbell, 2008).

2.1.1. Fatigue crack growth under variable amplitude loading

Fatigue crack growth under variable amplitude loading includes a load-interaction effect due to complicate loading. As referred by Schijve (1976), studies about crack growth under variable amplitude fatigue should include crack closure measurements. MacDougall and Topper (1997) found on fatigued notched steel AISI 1045 under variable amplitude loading ($R = -1$) that crack closure is reduced by periodic overloads. Sander and Richard (2005) also observed that overloads lead to retarded crack growth on fatigued alluminium alloy EN AW-7075-T651 under variable amplitude loading. Under block loading, they observed an acceleration of crack growth in low-high block loading and retardation in high-low block. Both retarded and accelerated crack growth were observed in low-high-low block. The retardation effect was studied by Pommier (2003) for fatigued 0,4% low carbon steel. He detected that retardation effect after consecutive overloads is larger that after a single overload, due to an adaptation of the material yield surface to the overload cycles.

2.2. Residual Stresses

2.2.1. Definition, Types and Origin

Residual Stresses are stresses remaining in materials without any external forces applied under uniform temperature conditions. Thus, they can be defined as self-equilibrating stresses.

Residual stresses can be classified as first, second, and third kinds (Macherauch, 1987):

- The 1st kind of residual stresses are nearly homogeneous in a macroscopic scale (across several grains) and are equilibrated within the whole body;
- The 2nd kind of residual stresses are nearly homogeneous in a microscopic scale (across one grain or parts of a grain) and are in equilibrium across a sufficient number of grains;
- The 3rd kind of residual stresses are inhomogeneous across submicroscopic areas of a material (several atomic distances within a grain) and are equilibrated across small parts of a grain.

All mechanical components have residual stresses resulting from the manufacturing processes, heat and mechanical treatments (Niku-Lari, 1987; Hauk et al., 1991). Residual stresses arise due to inhomogeneous elastic or plastic deformations that cause strain incompatibilities in a material during the manufacturing processes. Kloos and Kaiser (1991) describe the origin of residual stresses attributed to:

- partial plastic deformation of the surface zone caused by mechanical loading. Shot peening and deep rolling are processes that induce compressive residual stresses as a result of hardening processes;
- partial plastic deformation caused by inhomogeneous thermal loading, when the local thermal stresses exceed the yield limit of the material according to the corresponding temperature, leading to a partial plastic deformation. Such thermal stresses occur during quenching of components without phase transformation as a result of big temperature

differences between the core and the surface region that cause compressive residual stresses

- the interaction between the mechanical and thermal state of the material, in case of machining processes, due to the forces of the cutting tools causes at the surface zone compressive residual stresses with definite depths. Furthermore, due to the frictional contact between tool and work piece as well as high speeds of deformation that increase the temperature, tensile residual stresses can occur as well at the surface region;
- the interaction between the thermal and metallurgical state of the material, during the quenching of a heated component with phase transformation. This causes a superposition of residual stresses due to quenching and due to phase transformation which can lead to compressive or tensile residual stresses at the surface zone;
- the interaction between the mechanical, thermal and metallurgical state of the material in case of high-speed machining processes, particularly, in grinding with extremely high speeds which leads to a big thermal energy and, consequently, a martensite transformation occurs and tensile residual stresses are released below the surface. Its reduction from the surface region is result of a re-hardening zone and, thus, the involved increase of volume.

All these factors make the prediction of residual stresses very difficult when combined. The origin of residual stresses by machining, thermal and thermo mechanical surface treatments are detailed in Scholtes (1987) and in Ericsson (1987).

Another important and well-studied source of residual stresses is welding. Zinn and Scholtes (2002) stated that welding residual stresses are due to shrinkage processes which occur when heated and cooled zones are neighbored, due to quenching processes in the case of thicker plates when the near surface zones and the core layers are with considerable temperature differences during cooling processes, and due to phase transformations that can occur locally during the cooling period of the welded seam and cause volume changes.

Detailed description about generation of residual stresses due to welding is presented in Wohlfahrt (1987) and in Zinn and Scholtes (2002).

Usually, residual stresses are subdivided in two groups: the macrostresses, those which induce macroscopic dimensional changes and correspond to the first kind; and the microstresses, a combination of residual stresses from the second and third kind, and those are connected to the lattice imperfections within the grain or across the phase.

2.2.2. Induced residual stresses

2.2.2.1. Deep Rolling Process

Deep rolling is one of the mechanical surface treatments that induce high compressive residual stresses near the surface of technical components, which is very beneficial for the fatigue behaviour (Altenberger et al, 1999a). Other processes like shot peening or laser shock peening are well-known and were intensively studied (Macherauch and Hauk, 1987), however, in this work only deep rolling is presented, as well as, its influence in near surface alterations because it was the mechanical surface treatment used in this investigation. This process is a mechanical surface rolling treatment using rolls or ball-point tools with pressure to induce plastic deformations in the surface creating compressive residual stresses. The material deforms near surface, plastically, when the yield limit is exceeded by compressive mechanical loading and the compressive residual stresses appear due to elastic and plastic effects. Besides compressive residual stresses, deep rolling also induce strain hardening, These effects are function of the deep rolling parameters such pressure, feed rate, and geometry of the tool. Pressure is the most important parameter and only optimized pressures or rolling pressures have the desired effect on the fatigue behaviour, with too low pressures having no effect and too high ones aggravating the fatigue behaviour (Altenberger, 2005a). A typical residual stress distribution and FWHM values for AISI 1045 is shown in figure 8 for different deep rolling pressures. As can be seen the higher the pressure more stable are the residual stresses and the higher are the FWHM values below surface, showing the influence of deep rolling pressure on the affected depth.

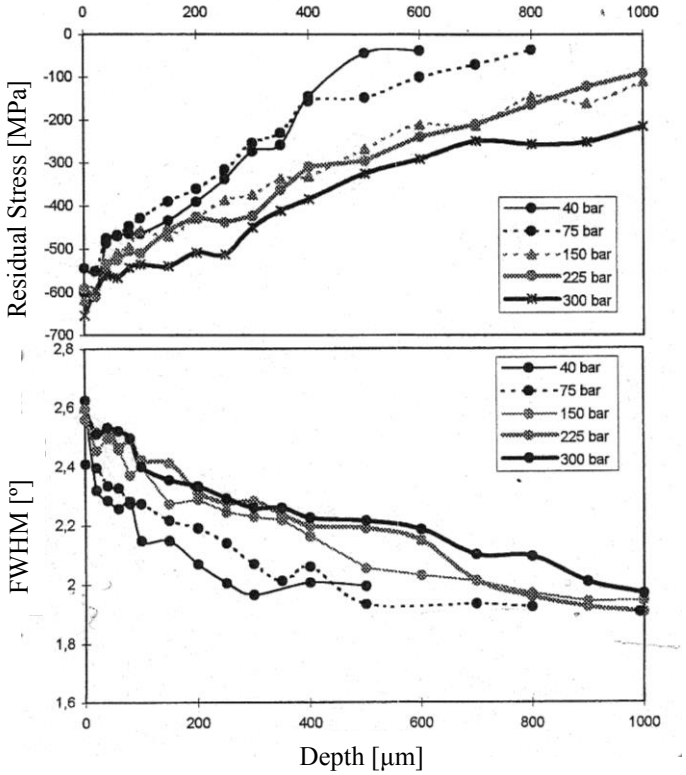

Figure 8 – Residual stress and FWHM depth profile of deep steel AISI 1045 for different deep rolling pressures (Altenberger, 2000).

Residual stress state in deep rolled materials also depends on material (Altenberger et al, 1999b). For the austenitic stainless steel AISI 304 and for the titanium alloy Ti-6Al-4V the maximum value of compressive stresses is below the surface (Altenberger, 2005b), but for the plain carbon steel AISI 1045 (figure 8) and for the aluminum alloy AA6110 the maximum value is near the surface (Juijerm et al, 2006).

Near-surface microstructure analysis of deep rolled materials can reveal different types of microstructures. Altenberger et al. (1999b) studied the microstrucures for different materials. It was identified for the stainless steel AISI 304 two layers in a complex microstructure: a nanocrystalline layer directly at the surface and a layer beneath the surface exhibiting very high dislocation densities. Both layers are partially martensitic. However, for the AISI 1045 steel only a simple dislocation cell structures were observed. Other different microstructures can be observed for the magnesium alloy AZ31 like deformation-twining structure.

Fatigue behaviour in surface treated materials can be enhanced by compressive residual stresses and work hardening. The depth of the layer which contains compressive

residual stresses and strain hardening also influences the fatigue behaviour depending which process are used and its parameters. This can be shown comparing the deep rolling process with the shot peened process that produces much higher surface roughness and affects less depth (Altenberger, 2005a). Residual stress depth profile for deep rolled AISI 304 presents higher values below the surface than shot peened, however, the maximum value belongs to shot peened material. The maximum FWHM value also is obtained for shot peened material that exhibits more work hardening near the surface than the deep rolled one. Even presenting higher strain hardening, the shot peened material exhibits higher plastic strain amplitude and lower fatigue lifetime that the deep rolled. Thus, can be proven that the plastic strain amplitude is rather governed by the surface treatment affected layer than by intensity of strain hardening. Also a higher surface roughness induced by an higher shot peening intensity exhibit lower fatigue life time since higher surface roughness presents more stress concentrations by notches. However, for similar mechanically surface treatment affected layers and residual stresses shot peened material exhibits better fatigue behaviour once it produces more cold work, as shown in Altenberger, (2003).

Deep rolling can be done with high temperatures (High Temperature Deep Rolling) which have a big influence on fatigue behaviour if optimized temperatures are used. Altenberger et al. (2005) studied the influence of temperature in deep rolling of the ferritic steel AISI 1045. It was found that an optimized deep rolling high temperature leads to higher compressive residual stresses near and below the surface and higher surface hardness than the conventional process, which improves fatigue behaviour. According to the authors, the better fatigue behavior is due to dynamic strain ageing, which stabilizes micro and macro residual stresses in near surface zones leading to improved surface hardness that prevents and delays crack initiation.

2.2.3. Measurement

2.2.3.1. X-ray Diffraction Method

The methods of residual stresses measurements can be divided in non-destructive and destructive methods. The most known methods are the hole-drilling method and the X-ray diffraction method. The hole-drilling method is a mechanical and destructive method and consists in opening a hole into a stressed body that relaxes the

stresses at that location. Normal stresses are eliminated at the hole boundary by the fact that the stress normal to any free surface must be zero, reducing the stresses in the surrounding region. This causes a redistribution of the local surface strains which measured provides the data to calculate the original residual stress state at the hole location. This method allows determining only residual stresses from the first kind (Niku-Lari et al., 1987).

While hole-drilling method measures the macroscopic surface strains, the non-destructive X-ray diffraction method measure homogeneous lattice strains in crystalline materials and determine residual stresses from the first and second kind (François et al., 1996). Lattice strains are the changes in lattice planes that are perfectly defined in crystalline materials, being a characteristic of the material. Thus, due to the regular distribution of atoms, when a monochromatic X-ray beam irradiates this type of material, it is scattered by the atoms leading to interferences similar to visible light diffraction by an optical diffraction pattern. The interferences are constructive if the Bragg´s law is fulfilled, that is, the diffracted beam and the incident beam are symmetrical in relation to the lattice planes normal, as represented in figure 9. The Bragg law is expressed in (2.12) where d is the distance between diffracting lattice planes, Θ is the angle between the incident beam and the diffracted planes, λ is the X-ray wavelength and n is an integer.

$$2dsin(\Theta) = n\lambda. \tag{2.12}$$

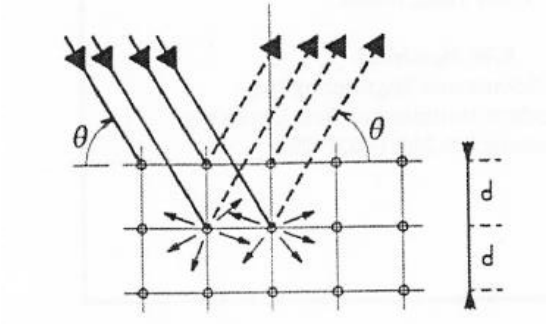

Figure 9 - Bragg law (François et al., 1996).

2.2.3.2. Strains measurement

For a given stressed specimen with d_0 as lattice spacing in free-stress state, due to elastic deformation, the lattice spacing d varies according to the orientation of planes

relatively to the stress direction (François et al., 1996). Independently of the stress direction, the lattice strain is given by:

$$\varepsilon = \frac{d - d_0}{d_0} = \frac{\Delta d}{d_0} = (\Theta - \Theta_0)cotg(\Theta_0) = -\Delta\Theta cotg(\Theta_0), \quad (2.13)$$

where Θ is the position of the diffraction peak corresponding to the lattice spacing d for stressed specimen and Θ_0 is the position corresponding to the lattice spacing d_0 for free-stressed specimen.

A diffraction peak is produced when the intensity recorded by the X-ray counter is increased as a result of an intersection of the counter and the diffracted beam. The diffracted beam is diffracted by specimen into cones as shown in figure 10a). A sketch of a diffractometer is given in figure 10b) showing how the measurement is done. A peak shift will be recorded as a result of lattice spacing changes only if it is homogeneous over all atoms and grains. However, the diffraction peak should be chosen at the highest angle Θ possible to obtain the largest peak shift $\Delta\Theta$ for a given lattice deformation. Figure shows diffraction peaks and peak shifts for high Θ angles 10c). The diffraction peak is recorded for each angle ψ which is the angle of the specimen as can be seen in figure 10b). Knowing the position of diffraction peak is possible to know the lattice spacing through Bragg law and plot the position against $sin^2\psi$ (François et al., 1996).

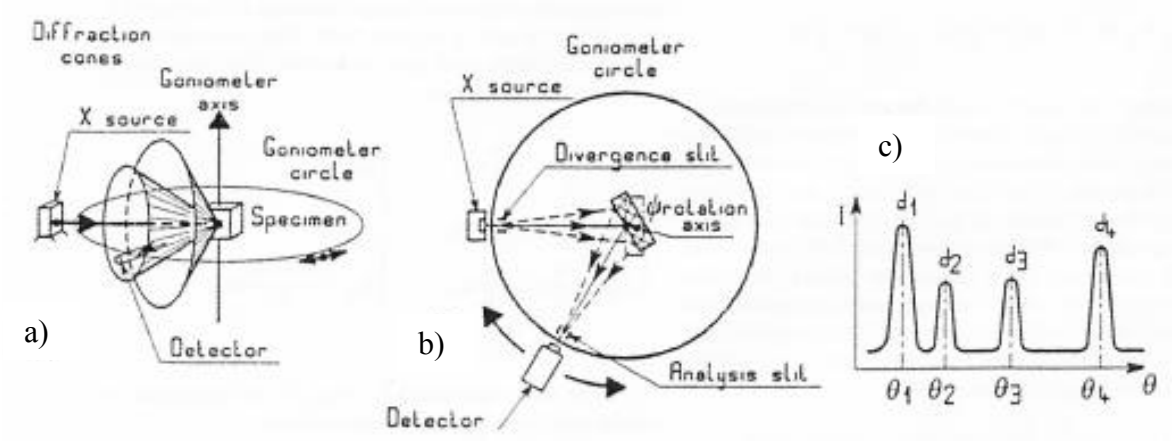

Figure 10 - Difractometer: a) Diffraction cones, b) Measurement, c) Resulting peaks (François et al., 1996).

2.2.3.3. Stresses determination from measured strains

Stresses can now be calculated once determined the strains for each ψ angle through equations of mechanics. Considering that the material is homogeneous, isotropic

and linear elastic (X-ray diffraction is only sensitive to elastic small deformation), stresses and strains can be related by (François et al., 1996):

$$\varepsilon_{ij} = \frac{1+\upsilon}{E}\sigma_{ij} - \frac{\upsilon}{E}\sigma_{kk}\delta_{ij}, \tag{2.14}$$

where E and υ are the Young´s modulus and the Poisson´s ratio of the material, respectively, and δ is the Kronecker´s symbol.

In a uniaxial stress state, and considering a reference frame (S_1, S_2, S_3) in a specimen subjected to a stress σ_{11} along direction s_1, the nonzero strain tensor components are ε_{11}, ε_{22}, and ε_{33}. From figure 11, that shows the deformation of the specimen under a uniaxial stress σ_{11}, the projection of the strain tensor on direction *n* which is described by ψ angle gives us the strain ε_{ψ} expressed by σ_{11} (François et al., 1996).

$$\varepsilon_{\psi} = \frac{1+\upsilon}{E}sin^2\psi.\sigma_{11} - \frac{\upsilon}{E}\sigma_{11} = \frac{1}{2}S_2\{\text{hkl}\}sin^2\psi.\sigma_{11} + S_1\{\text{hkl}\}.\sigma_{11}, \tag{2.15}$$

where $1/2\ S_2\{\text{hkl}\}$ and $S_1\{\text{hkl}\}$are elastic constants commonly used in the field of X-ray depending on the lattice plane {hkl}on which the measurement is performed

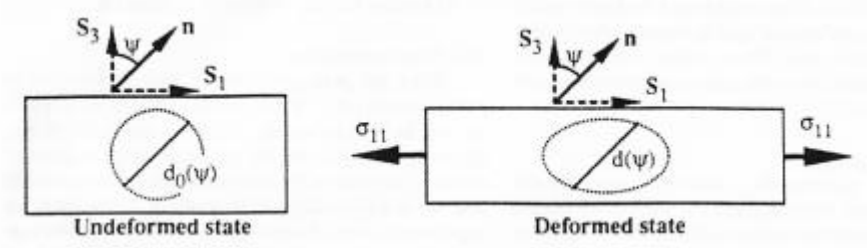

Figure 11 – Specimen subjected to a uniaxial stress σ_{11} (François et al., 1996).

Stress determination becomes three-dimensional in the case of biaxial stress state, therefore, the projection of the strain tensor on direction *n* is now described by two angles Φ and ψ, as can be seen in figure 12. The nonzero stress tensor components are σ_{11}, σ_{12}, and σ_{22}. Thus, the measured strain is:

$$\varepsilon_{\phi\psi} = \frac{1+\upsilon}{E}(\sigma_{11}cos^2\phi + \sigma_{12}sin2\phi + \sigma_{22}sin^2\phi)sin^2\psi - \frac{\upsilon}{E}(\sigma_{11}+\sigma_{22}). \tag{2.16}$$

In terms of elastic constants and substituting the term between the first parentheses by the stress value σ_{Φ} along L´$_1$ and the term between the second parentheses by the trace of tensor σ the expression (2.17) becomes:

$$\varepsilon_{\phi\psi} = \frac{1}{2}S_2\{\text{hkl}\}\sigma_{\phi}sin^2\psi + S_1\{\text{hkl}\}Tr(\sigma). \tag{2.17}$$

It can be seen from the equation (2.17) that the slope is proportional to σ_ϕ ant the intercept is proportional to the trace of the stress tensor.

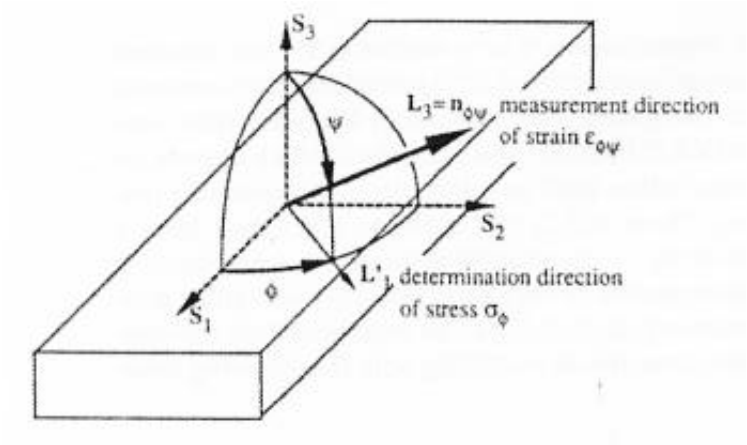

Figure 12 - Schematic representation of measurement and determinations directions of stresses and strains in a 3-dimensional system (François et al., 1996).

The case of a triaxial stress state is treated similarly to the biaxial case. In this case is necessary to determine the full stress tensor, so the measured strain is given by (François et al., 1996):

$$\varepsilon_{\phi\psi} = \frac{1+\upsilon}{E}(\sigma_{11}cos^2\phi + \sigma_{12}sin2\phi + \sigma_{22}sin^2\phi - \sigma_{33})sin^2\psi + \frac{1+\upsilon}{E}(\sigma_{13}cos\phi + \sigma_{23}sin\phi)sin2\psi + \frac{1+\upsilon}{E}\sigma_{33} - \frac{\upsilon}{E}(\sigma_{11} + \sigma_{22} + \sigma_{33}). \quad (2.18)$$

In a condensed way using the same substitutions for the biaxial stress state and substituting the term between the third parentheses by the shear stress in direction ϕ (François et al., 1996):

$$\varepsilon_{\phi\psi} = \frac{1}{2}S_2\{\text{hkl}\}(\sigma_\phi - \sigma_{33})sin^2\psi + \frac{1}{2}S_2\{\text{hkl}\}\sigma_{33} + S_1\{\text{hkl}\}Tr(\sigma) + \frac{1}{2}S_2\{\text{hkl}\}\tau_\phi sin2\psi. \quad (2.19)$$

2.2.3.4. Full width at half maximum value

The full width at half maximum value is the distance between two points corresponding of the width of the peak at the half maximum height position as shown in figure 13. This value is sensitive to the variation in microstructure and stress-strain accumulation in the material. FWHM can be used as an indicator of work hardening since it affects the crystallinity and grain boundary mobility, which in turns causes a linear increase in the FWHM of X-ray peak (Vashista and Paul, 2012).

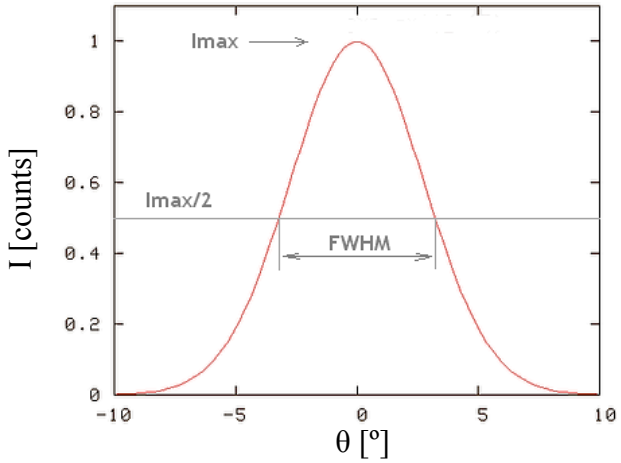

Figure 13 - Example of a peak and the full width at half maximum value (Scientific Volume Imaging, 2013).

2.3. Effects of mechanically surface treated zone on fatigue behavior

2.3.1. Residual stresses relaxation

Effects of residual stresses on fatigue behaviour were largely studied and it is well-established that compressive residual stresses improve fatigue lifetime, whilst tensile residual stresses have the opposite effect. Fatigue behaviour enhancement depends on residual stresses stability because they get partially or completely relaxed during fatigue life. Residual stress relaxation due to cyclic loading is influenced mainly by (Zhuang and Halford, 2001): initial magnitude and gradient of the residual stress field and degree of cold working; fatigue stress amplitude, mean stress ratio and number of cycles; and material cyclic stress-strain response and degree of cyclic work hardening/softening. The

main relaxation takes place in first cycles when long ranged macro-stresses vanish, followed by further gradual relaxation during life time when cyclic softening sets in and short-ranged residual stresses are decreased by microstructural effects (Martin et al., 1998). Martin et al. (1998) studied the cyclic deformation behaviour for shot peened AISI 1045

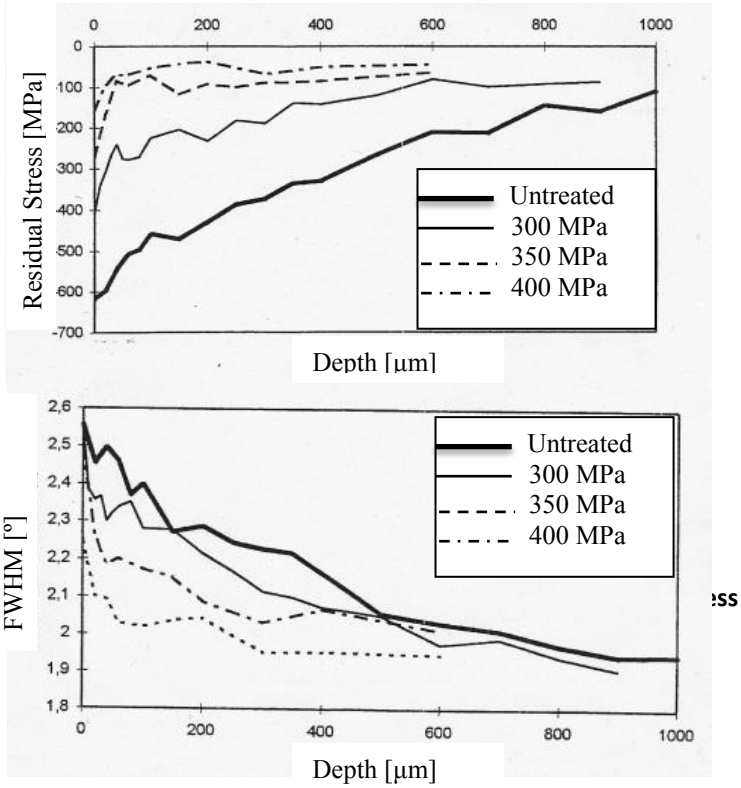

and observed a strong correlation between residual stress relaxation and development of plastic strain amplitude during fatigue, which is stronger for the highest stress amplitude used of 450 MPa. Dalaei et al. (2011) also stated that the stability of residual stresses is determined by plastic strain amplitude and number of cycles during the fatigue loading.

Altenberger et al. (1999) compared cyclic deformation behaviour of steel AISI 1045 with the austenitic steel AISI 304 and with the magnesium alloy AZ 31. It was found a different stability of macrostresses, microstresses and near surface microstructures for the three materials. Macrostresses represented by residual stresses depth profiles were drastically or completely relaxed during fatigue loading. However, behaviour of FWHM values that represent microstresses was distinctly different. It was observed for steel AISI 1045 that FWHM was severely diminished by fatigue, while total stability was found for AISI 304 and AZ 31. This behaviour is due to different stability of near surface microstructures during fatigue and, consequently, leads to an improvement of fatigue

lifetime in AISI 304 and in AZ 31 and no improvement in AISI 1045. Typical residual stress and FWHM values distributions for deep rolled ($P = 150\ bar$) AISI 1045 are shown in figure 14. In figure 15 is exhibited the influence of stress amplitude and deep rolling pressure on cyclic deformation behaviour of steel AISI 1045.

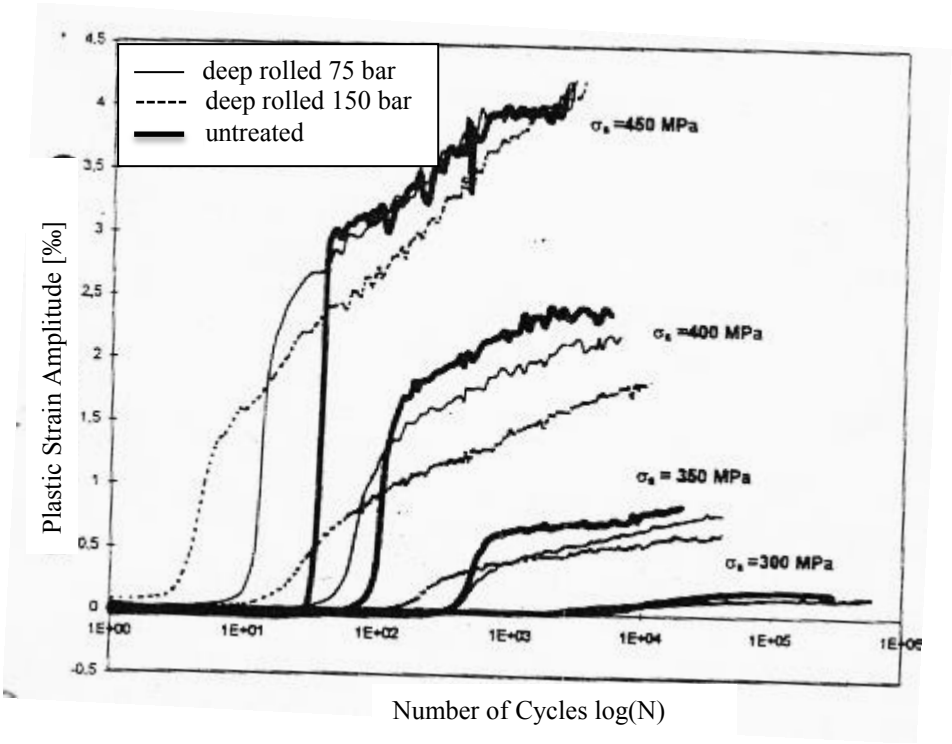

Figure 15 – Influence of stress amplitude and deep rolling pressure on cyclic deformation behaviour of steel AISI 1045 (Altenberger, 2000).

2.3.2. Effects on fatigue crack initiation and propagation

During cyclic loading, cracks arise as a result of microstructural changes at stress concentration points. The number of cycles to crack initiation can be extended by mechanically surface treated zones once these treatments induce work hardening and compressive residual stresses. Also, they can be also shortened by shot peening due to the high surface roughness and micro-notches produced (Eifler et al., 1991). However the effects of residual stresses are very difficult to predict due to the difficulties related to observation of microcracks. It is known that work hardening leads to an increase of number of cycles to crack initiation since it is an obstacle to crack initiation mechanisms. For residual stresses, few works were found in this field. Almer et al. (2000) found that macrostresses have influence on the number of cycles to crack initiation in press-fitted steel AISI 1080. The material, polished and double-edge notched was subjected to high

cycle fatigue and crack initiation was monitored by surface replicas. The local stress–strain behavior in the vicinity of the initiation sites was tracked using finite element analysis. It was observed a rapidly relaxation of microstresses, while macrostresses remained stable throughout fatigue life and increased number of cycles to crack initiation.

Fatigue performance can be assessed using macro crack growth behaviour when residual stresses depths are large such as in the case of deep rolling process. Fatigue crack propagation is slow in the beginning of the crack, but increases with the increasing crack length. Usually, fatigue crack growth can be analyzed in terms of linear elastic fracture mechanics by the crack growth rate da/dN against the stress intensity factor range ΔK. Figure 16 shows a curve representative of fatigue crack growth where three regions are observed. In region I, ΔK_{th} is the threshold stress intensity factor below which measurable crack growth is not detected. Region II, presents a linear crack growth that can be described by Paris equation (Campbell, 2008):

$$\frac{da}{dN} = C\Delta K^m, \tag{2.20}$$

where *a* is the crack size, *N* is the number of cycles, *C* and *m* are material parameters, and ΔK is given by the difference between maximum K_{max} and minimum K_{min} stress intensity factors applied during the load cycle.

An increase in stress ratio $R = K_{min}/K_{max}$ has the effect of moving regions I and II to lower ΔK values. The presence of residual stresses can alter *R* and also ΔK value, over which the crack remains open. Thus, applying the principle of superposition an effective stress intensity factor range can be defined (Campbell, 2008):

$$\Delta K_{eff} = K_{max}^{eff} - K_{min}^{eff}, \tag{2.21}$$

where the effective maximum and minimum stress intensity factors, K_{max}^{eff} and K_{min}^{eff} can be calculated by:

$$K_{max}^{eff} = K_{max} + K_{res}, \tag{2.22}$$

$$K_{min}^{eff} = K_{min} + K_{res}, \tag{2.23}$$

where K_{res} is the stress intensity factor due to residual stresses distribution. Therefore, for a minimum effective stress intensity factor $K_{min}^{eff} > 0$, effective stress intensity factor range ΔK_{eff} and the effective stress ratio R_{eff} are given by:

$$\Delta K_{eff} = K_{max}^{eff} - K_{min}^{eff} = K_{max} - K_{min}, \tag{2.24}$$

$$R_{eff} = \frac{K_{min}^{eff}}{K_{max}^{eff}} = \frac{K_{min} + K_{res}}{K_{max} + K_{res}}. \tag{2.25}$$

As can be seen, ΔK_{eff} depends only on the nominal stress applied and only R_{eff} is affected by residual stresses, since the crack faces will always remain open throughout a cycle. When $K_{min}^{eff} < 0$, both factors are affected (Glinka, 1987) by equation and the follow:

$$\Delta K_{eff} = K_{max} + K_{res}, \tag{2.26}$$

which means that the crack will be closed for part of the cycle. With this approach fatigue crack growth is given by (Campbell, 2008):

$$\frac{da}{dN} = C\Delta K_{eff}^{m}. \tag{2.27}$$

In general, tensile residual stresses increase fatigue crack growth rate and decrease fatigue life, however its influence on fatigue life is less than the influence of compressive residual stresses have on fatigue life increase by an equal value of residual stresses (Glinka, 1987). Compressive residual stresses should have most influence on fatigue crack growth when $K_{min} < |K_{res}|$.

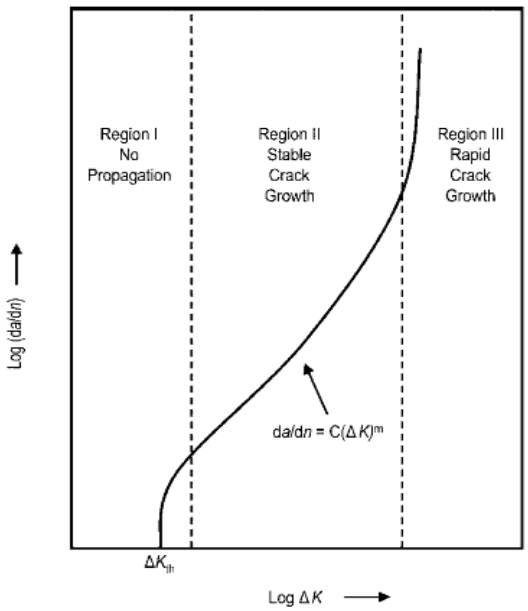

Figure 16 - Crack propagation curve for fatigue loading (Campbell, 2008).

3. METHODOLOGY

This work was carried out at the Institute of Materials Science, Metallic Materials, University of Kassel, between April and August of 2013.

Initially, the samples were deep rolled to induce compressive residual stresses. Secondly, fatigue tests were performed in order to study the stability of residual stresses after cyclic loads. Thirdly, residual stresses were measured at and beneath the surface using X-ray diffraction. Electrolytic Polishing was used to remove parts of the material. Finally, the hardness of the specimens was measured regarding the correlation between strain hardening and stability of residual stresses with the cyclic deformation behaviour. In the next subchapters the parameters of each process are explained.

3.1. Material

The cylindrical specimens made of plain carbon steel SAE 1045 (German Grade Steel Ck45) have the geometry presented in figure 17. The chemical composition is given in table 1. The mechanical properties were determined for the same steel by Martin et al. (1998) that revealed yield strength of 460-480 MPa, ultimate tensile strength of 740 MPa, and elongation of 22%.

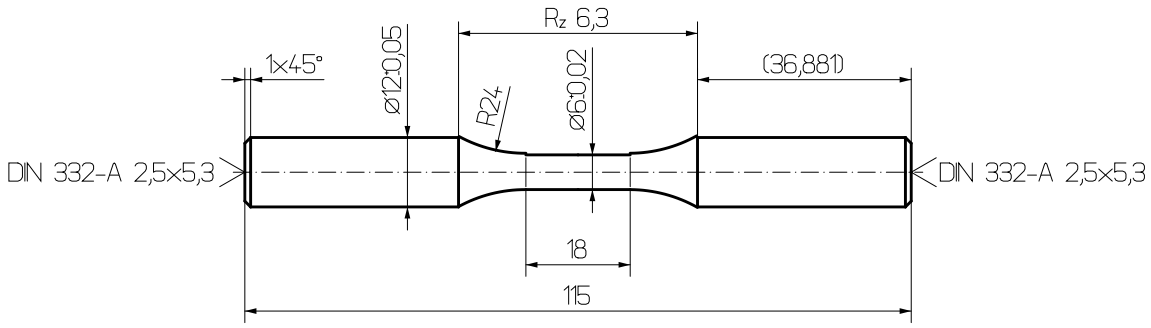

Figure 17 - Geometry of the specimen [mm].

Tabel 1 - Chemical composition of AISI 1045 (Martin et al., 1998).

Element	C	Si	Mn	P	S	Fe
wt.%	0.45	0.21	0.64	0.02	0.03	Rest

3.2. Deep rolling parameters

Deep rolling process was used to induce compressive residual stresses in near surface regions of the specimen. The specimen placed in a turning machine with a speed of 80 rpm was subjected to hydrostatic pressure in the surface in a longitudinal direction with a feed of 0,0995 mm. The hydrostatic pressure was applied for a ball-point device with 6.6 mm diameter represented in figure 18 and it was created by hydraulic pressure of 100 bar.

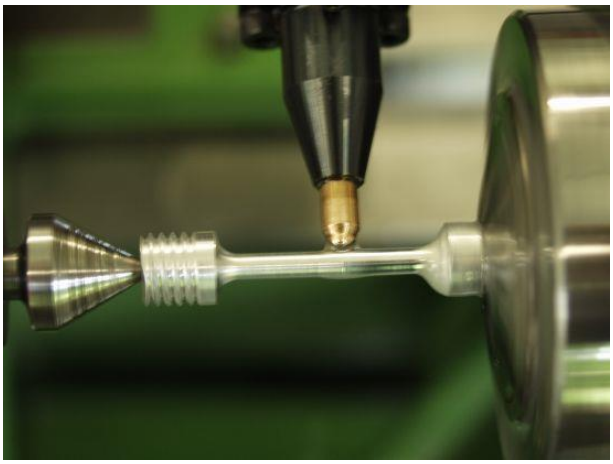

Figure 18 – Ecoroll HG6-19 device used in deep rolled (University of Kassel).

3.3. Fatigue test parameters

Tension/Compression fatigue tests were performed on a servo-hydraulic test system Schenck Hydropulser® 63 kN under load control. This system can apply loads until 63 kN and the data was collected by MTS 793 software. Three stress amplitudes of 300, 350 and 400 MPa were defined, the low (L), basic (B) and high amplitude (H), respectively. Fatigue tests were realized with these stress amplitudes without mean stresses ($R = -1$) at room temperature ($\approx 25^{o}$C) and a frequency of 5 Hertz. Initially, specimens were subjected to fatigue until failure in order to determine half of cycles to failure (N_f /2). Secondly, half of cycles to failure were applied regarding residual stresses measurement.

The fatigue tests performed are given in table 2 and table 3. These tables give the load sequences used, that is, which stress amplitude was applied (L, B, or H). For example, a load sequence B – L means that was used basic amplitude followed by low amplitude.

Tabel 2 – Load sequences performed in fatigue tests.

Load Sequence	Stress Applied [MPa]	Number of Cycles Applied	RS Measurement	Name of Load Sequence
L	300	463 127	No	Low
B	350	24 929	No	Basic
H	400	4 439	No	High
L	300	231 500	Yes	N_Low/2
B	350	12 500	Yes	N_Basic/2
H	400	2 220	Yes	N_High/2
B – L	350 - 300	12 500 – 42 762	No	N_Basic/2 + N_Low
B – H	350 - 400	12 500 – 3 325	No	N_Basic/2 + N_High
B – L	350 - 300	12 500 – 21 381	Yes	N_Basic/2 + N_Low/2
B - H	350 - 400	12 500 - 1662	Yes	N_Basic/2 + N_High/2
B – L	350 - 300	12 500 – 1 000	Yes	N_Basic/2 + 1000_Low
B – H	350 - 400	12 500 – 1 000	Yes	N_Basic/2 + 1000_High
B – L	350 - 300	100 – 822 273	No	100_Basic + N_Low
B – H	350 - 400	100 – 4 606	No	100_Basic + N_High
B – L	350 - 300	100 – 411 086	Yes	100_Basic + N_Low/2
B – H	350 - 400	100 – 2 303	Yes	100_Basic + N_High/2

Moreover, half of one cycle was applied after N_f /2 cycles of basic amplitude. Half cycle was applied in tension (T) and in compression (C) for high and low amplitudes as given in table 2.

Tabel 3 - Load sequences performed in variable amplitude loading fatigue tests with half cycle.

Load Sequence	Stress Applied [MPa]	Number of Cycles Applied	RS Measurement	Name of Load Sequence
B – H	350 – 400	12 500	Yes	N_Basic/2 + Tension_High
B – H	350 - 400	12 500	Yes	N_Basic/2 + Compression_High
B – L	350 – 300	12 500	Yes	N_Basic/2 + Tension_Low
B – L	350 - 300	12 500	Yes	N_Basic/2 + Compression_High

After fatigue tests, collected data were analyzed and hysteresis calculations were done in the software HysCalc® version 2.02 provided by University of Kassel. Figure 20 shows the equipment utilized. An extensometer with a measure length of 15 mm was used to measure the deformations as represented in figure 19.

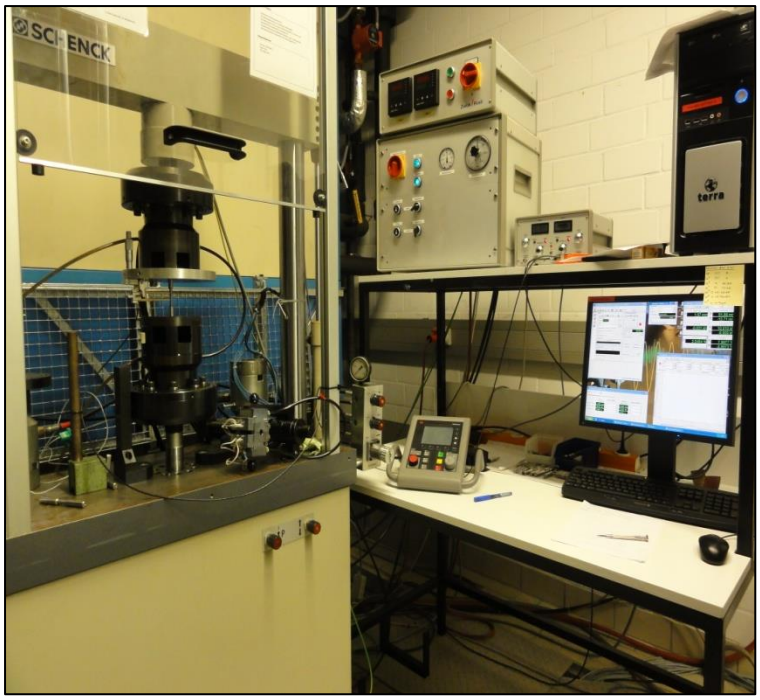

Figure 19 – Equipment used in fatigue tests (University of Kassel).

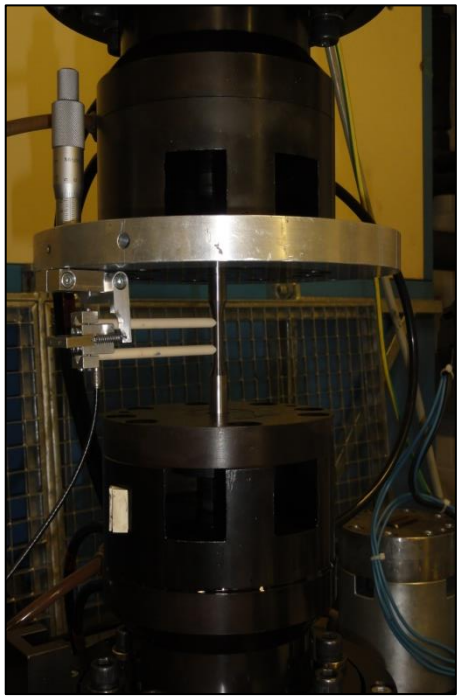

Figure 20 – Extensometer, specimen, and the bottom and top grip from the servo-hydraulic system used (Univesity of Kassel).

3.4. X-ray diffraction parameters

Residual stresses were measured by X-ray diffraction on a diffractometer Siemens D5000 exhibited on figure 21. All measurements were carried out with CrK_{α_1}

radiation with $\lambda = 2{,}2897263 \times 10^{-10}$ m. Measurements were done between 148° and 164° of 2Θ with a step size of 0,1° and 1 second per step. Tilting of specimen ψ ranged between -45° and + 45°. Peak calculations of the {211}-Bragg peak were carried out with the software Stress® version 1.04 using the sliding gravity method. Stresses calculations were done with the classical $sin^2\psi$ method. Constants used in calculations were the following:

$$2\Theta = 156{,}07^o$$

$$S_1 = -1{,}3333E^{-6}\ 1/MPa$$

$$\frac{1}{2}S_2 = 6{,}09E^{-6}\ 1/MPa$$

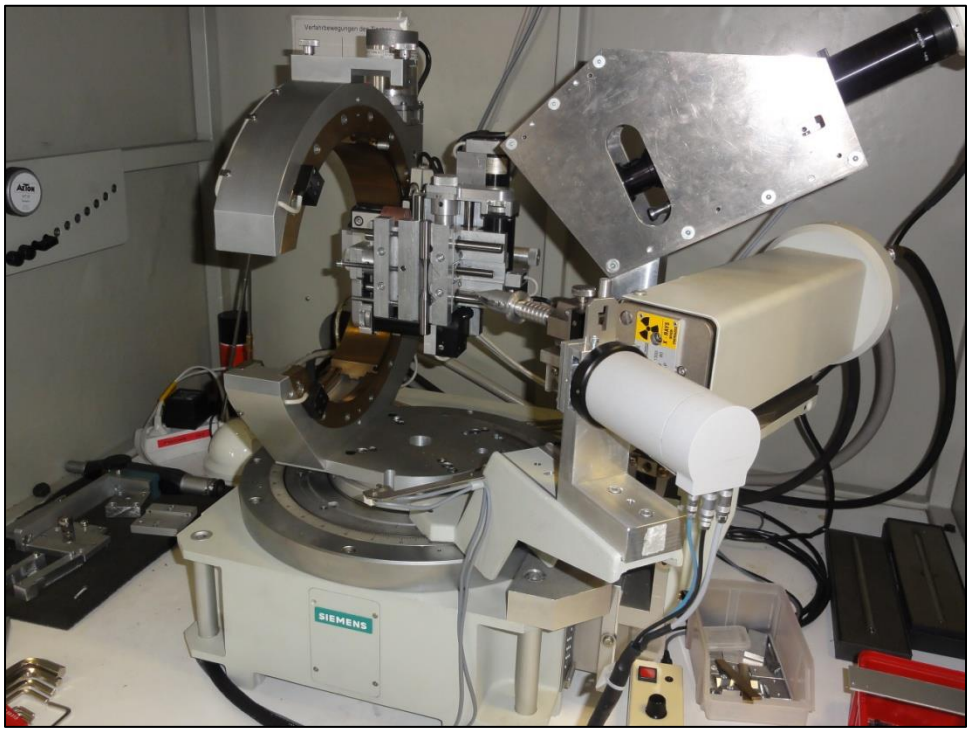

Figure 19 – Diffractometer Siemens D5000 used in X-ray diffraction (University of Kassel).

3.5. Electropolishing process

This process was used to remove material as specified in figure 22. Electrolytic removal was carried out in a fully automatic polisher Kristall 620® by ATM. In this process, material is removed due to its dissolution in the electrolyte caused by a passage of an electric current. This process does not induce residual stresses. The work piece is the anode which is connected to the positive terminal of the direct current power supply. The

negative terminal is connected to the cathode usually made of stainless steel, copper or lead. The work piece (anode) and the cathode are immersed into the electrolyte, and together with the DC power supply form an electric circuit. Therefore, as a result of electric current passage, atoms of material are converted to ions and removed from material surface as an insoluble precipitate. Figures 23 and 24 show the equipment utilized.

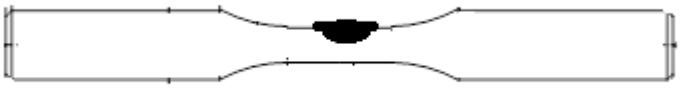

Figure 20 – Removed material in the specimen.

Figure 23 – Equipment used in electropolishing (University of Kassel).

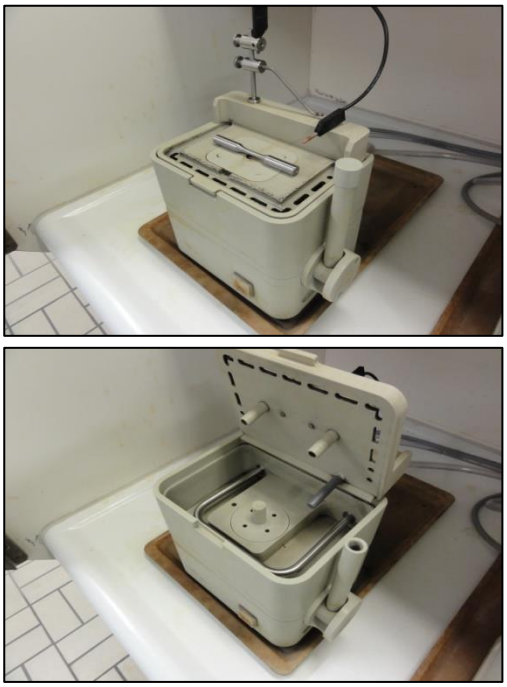

Figure 24 – Polishing unit used in electropolishing (University of Kassel).

3.6. Microhardness measurement

3.6.1. Specimen preparation

Before hardness measurement, a cross section of the specimen must be prepared. Samples to measure the hardness were cut from the original specimen in the transversal direction in order to obtain hardness depth profiles. Cutting was carried out

with a diamond blade in IsoMet® 1000 Precision Saw from Buehler. Water and cutting fluid (Buehler Cool 2) were used as cooling fluids.

Then, samples were embebbed into a cylindrical resin body with 40 mm diameter on an automatic mounting press SimpliMet® 1000 from Buehler. Pressure of 200 bar and temperature of 180^{o}C were used. Buehler PhenoCure® Black was the compression mounting compound utilized.

Finally, samples were ground and polished on a grinding and polishing automatic machine Buehler Phoenix® 4000. Initially samples were ground on a sandpaper with the following grain size: 75, 60, 45, 25, 15, 10 and 5 μm. After, they were polished with a policrystalline diamond suspension MetaDi® Supreme by Buehler with 3 and 1 μm of grain size. To finish the surface, Buehler MasterPrep® Polishing Suspension 0,05 μm was employed. Figure 25 illustrates one final embebbed sample after surface treatment.

Figure 21 – Cross section into a resin body with 40 mm of diameter.

3.6.2. Microhardness test parameters

Microhardness measurements were carried out on Fischerscope® HM2000, a microhardness measurement system that uses the load/indentation depth method according to ISO 14577-1. In this method, an indentation is created by an indenter which is pressed into the material with an increasing load and then unloaded. The Vickers indenter is made of diamond and has a shape of a pyramid. During indentation, the depth of indentation h is measured and plotted against force of the indenter F. This data allows to calculate Martens

hardness $HM = F/A$ where the surface of indentation $A = f(h)$. Calculations were done by the software WIN-HCU® version 6.5.

In this work, load test was increased during 20 s until reach the maximum load of 300 mN. Then maximum load was kept constant during 5 s. After this, specimen was unloaded during 20 s. Martens Hardness (HM [MPa]), Vickers hardness (HV) and maximum indentation depth (h_{max} [μm]) were measured by the software in several points starting from the side opposite to removed material side. That is, the side with deep rolled characterisitcs. Figure 26 shows a scheme of measurement points.

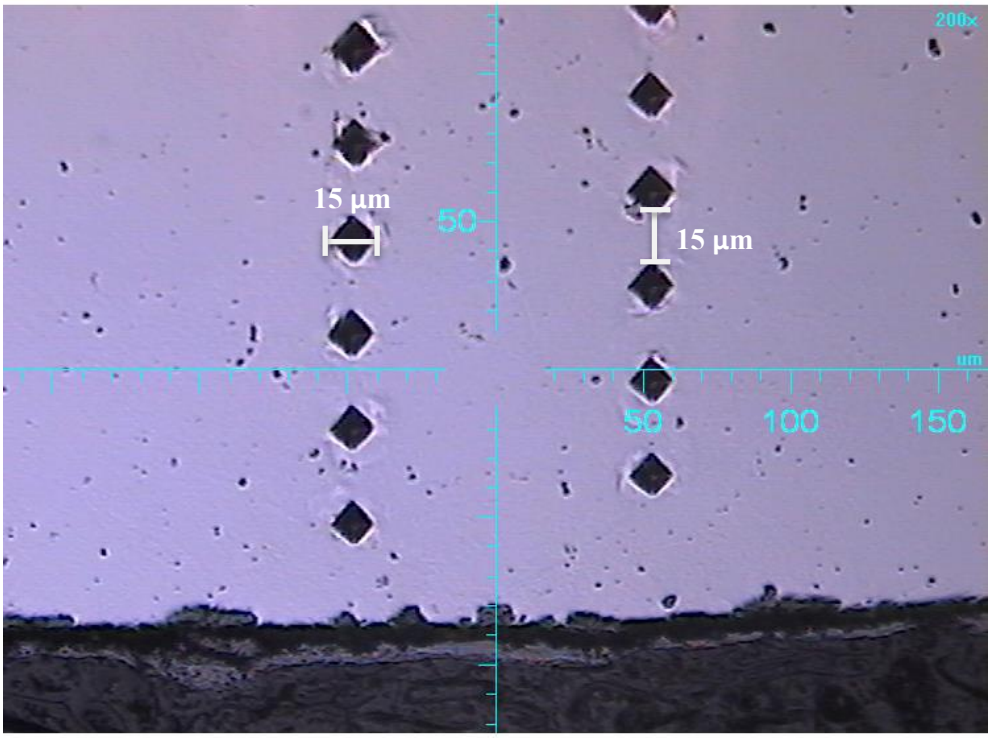

Figure 22 – Indentations for microhardness measurement.

4. RESULTS

In this section results are presented. Residual stresses, full width at half maximum values (FWHMV) and hardness depth profiles are shown as well as plastic strain amplitude curves in order to evaluate cyclic deformation behaviour.

4.1. Near surface zone properties

During fatigue, relaxation of residual stress occurs which depends on fatigue load as referred. Figures 23 and 24 show the residual stress distribution and FWHM values for the different load amplitudes used after half of cycles to failure. It corresponds to 12500 cycles for the basic amplitude, 2220 cycles for the high amplitude and 231 500 for the low amplitude. As can be seen higher relaxation occurs for the highest load amplitude of 400 MPa. The value for compressive residual stress at the surface differs in 67 % between the highest and the lowest load amplitude which also shows more stability. FWHM are in accordance with the residual stress distribution. The highest FWHM value that represents the highest value of hardness at the surface is shown for the lowest load amplitude proving that less residual stress relaxation occurred. For a deep rolled non-fatigued specimen a high value of compressive residual stress is observed near the surface remaining stable showing the effect of the mechanical surface treatment. The difference of compressive residual stress near the surface between the fatigued with the basic load amplitude and non-fatigued specimen is about 78 %. Hardness-depth profiles in figure 25 shows the effect of stress amplitude. on softening of material.

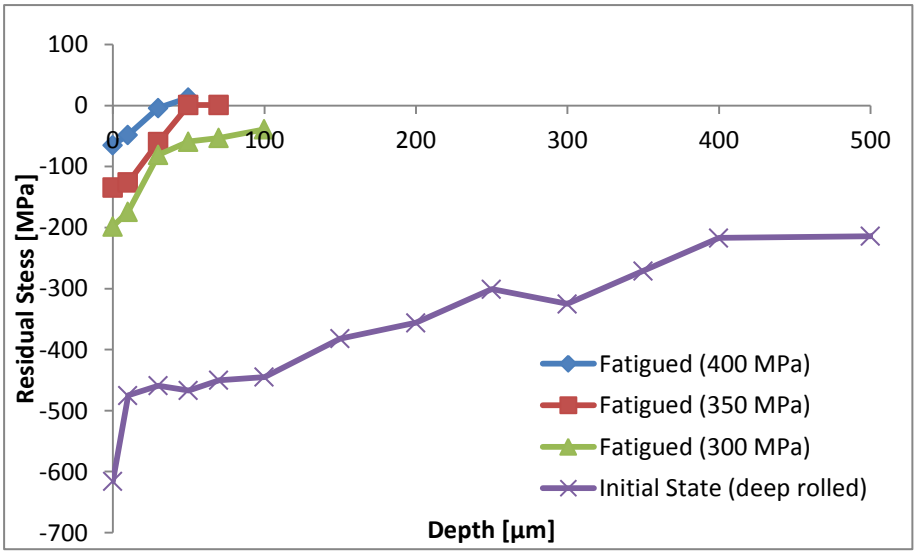

Figure 23 – Residual stress depth profile for fatigued and non – fatigued specimens.

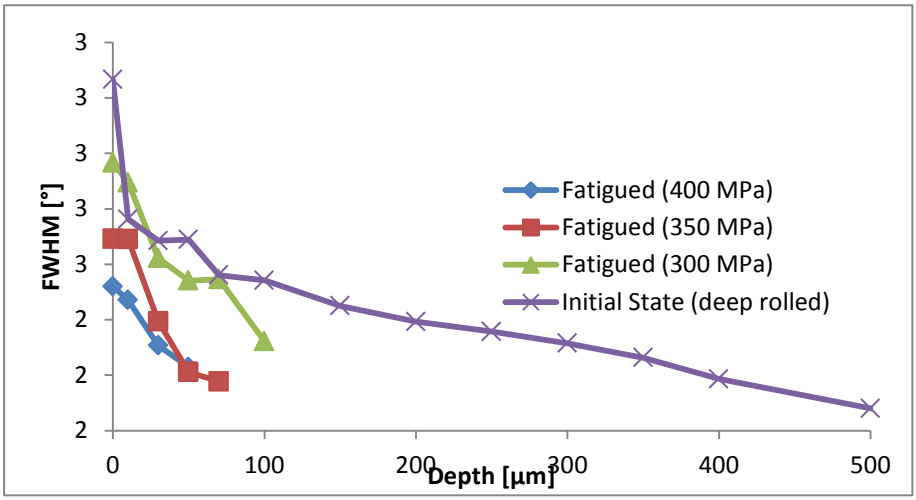

Figure 24 - FWHM depth profile for fatigued and non – fatigued specimens.

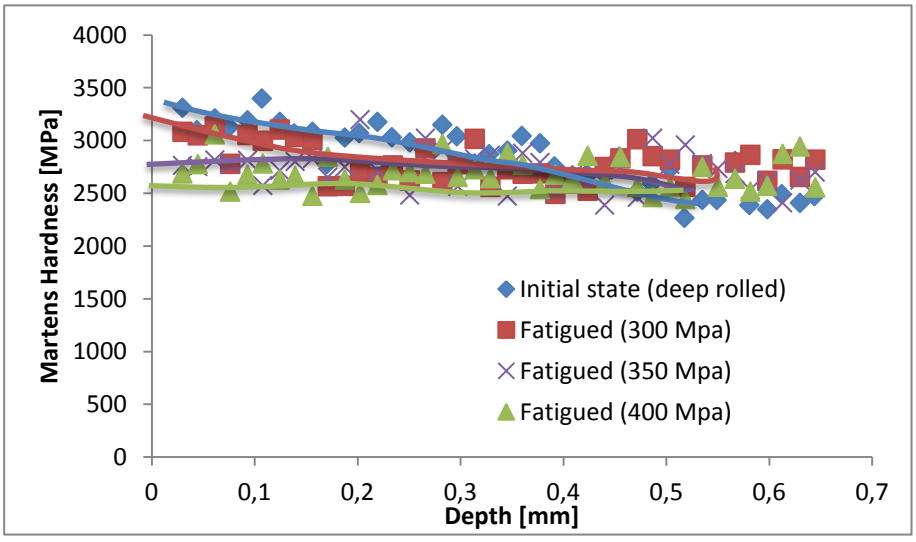

Figure 25 - Hardness depth profile for fatigued and non – fatigued specimens.

For multi-level loads the results are the following. Two load sequences of different stress amplitudes were used. The first was with half cycles of fracture of the basic load amplitude plus 1000 cycles of the low load amplitude. The second was with half cycles of fracture of the basic load amplitude plus 1000 cycles of the high load amplitude. No significant influence is observed as can be seen in figures 26 and 27. Similar values of compressive residual stresses at the surface are observed as well as similar residual stresses and FWHMV distribution. Figures 29 and 30 exhibit residual stress and FWHMV depth profiles after fatigue tests with half cycles of fracture for basic load amplitude plus half of the cycles for low load amplitude (21 381 cycles) and for high load amplitude (1662 cycles). Near the surface compressive residual stress value is similar for both load sequences, however, they exhibit a different distribution. As can be seen after the high load amplitude compressive residual stresses are quickly and completely relaxed in a shorter distance from surface, while after the low load amplitude they present much more stability. Hardness depth profiles are shown in figures 28 and 31 showing accordance with FWHM values.

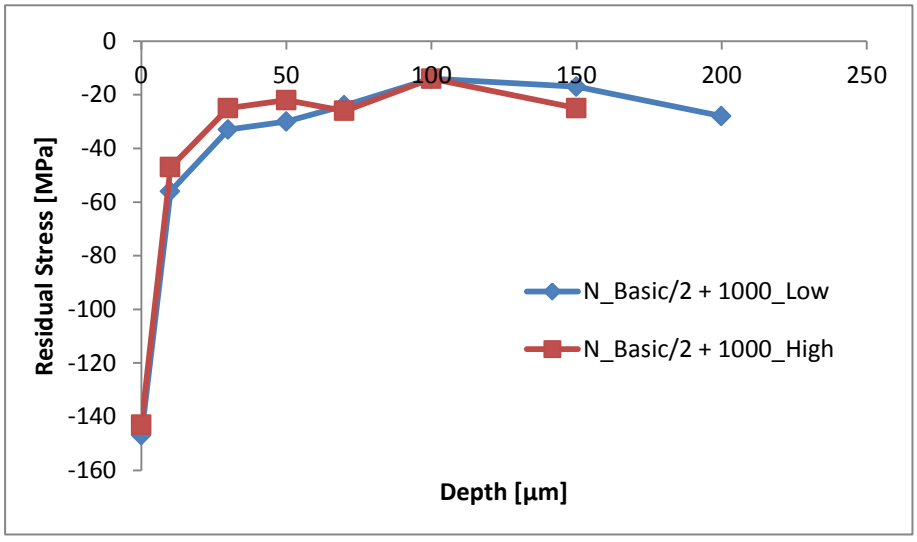

Figure 26 - Residual stress depth profile for sequences N_Basic/2 + 1000_Low and N_Basic/2 + 1000_High.

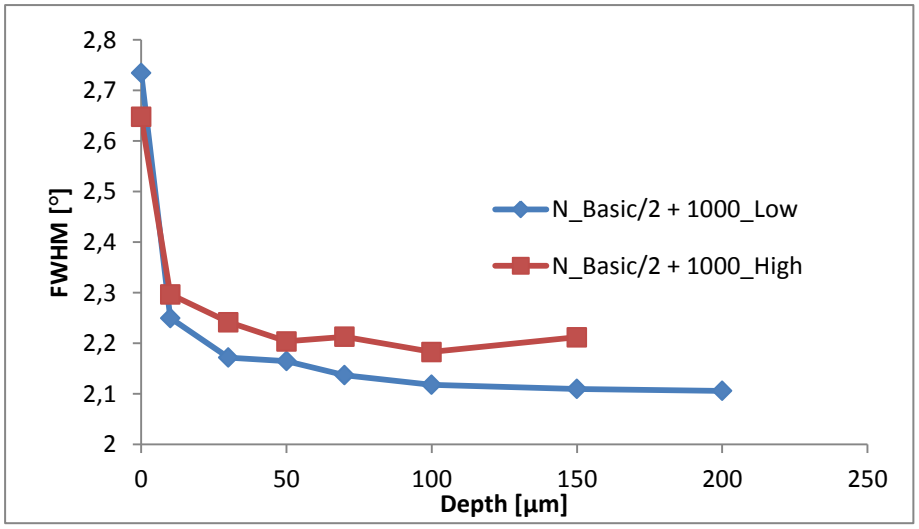

Figure 27 FWHM depth profile for sequences N_Basic/2 + 1000_Low and N_Basic/2 + 1000_High.

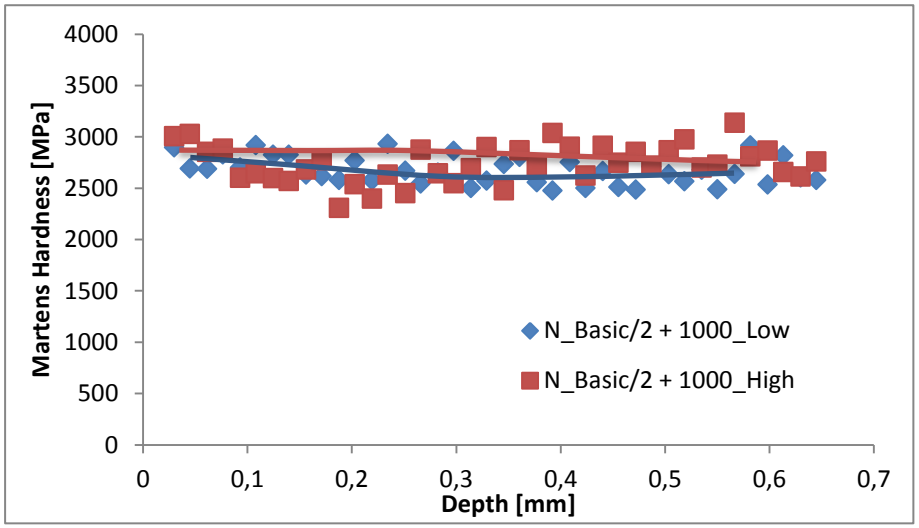

Figure 28 – Hardness depth profile for sequences N_Basic/2 + 1000_Low and N_Basic/2 + 1000_High.

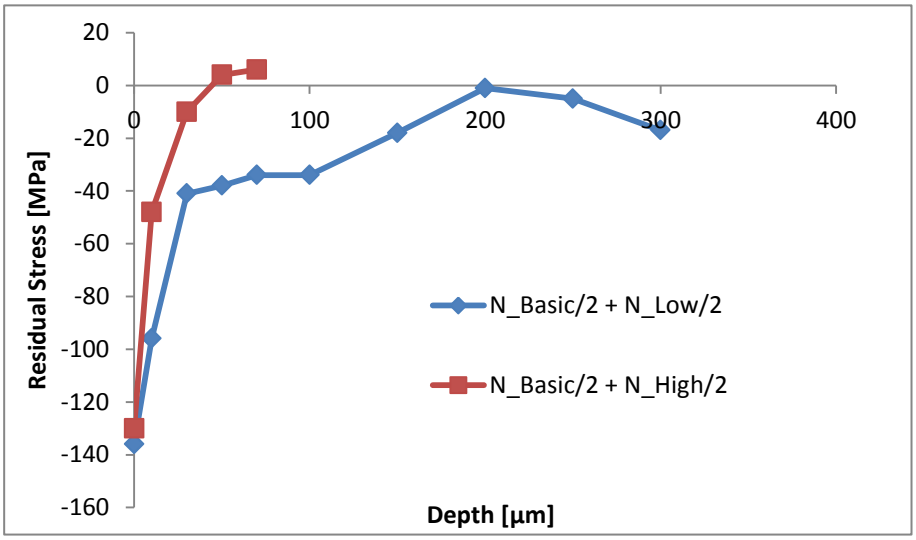

Figure 29 - Residual stress depth profile for sequences N_Basic/2 N_Low/2 and N_Basic/2 +N_High/2.

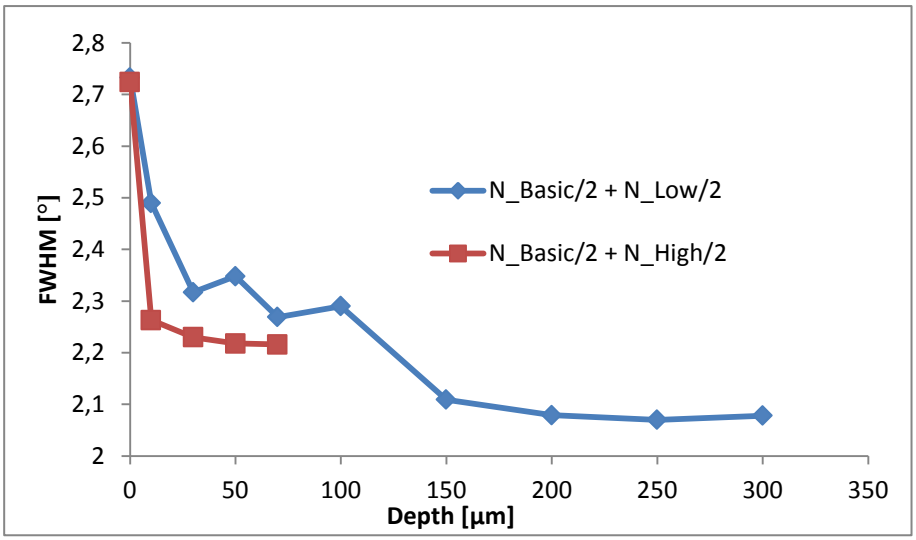

Figure 30 – FWHM depth profile for sequences N_Basic/2 N_Low/2 and N_Basic/2 +N_High/2.

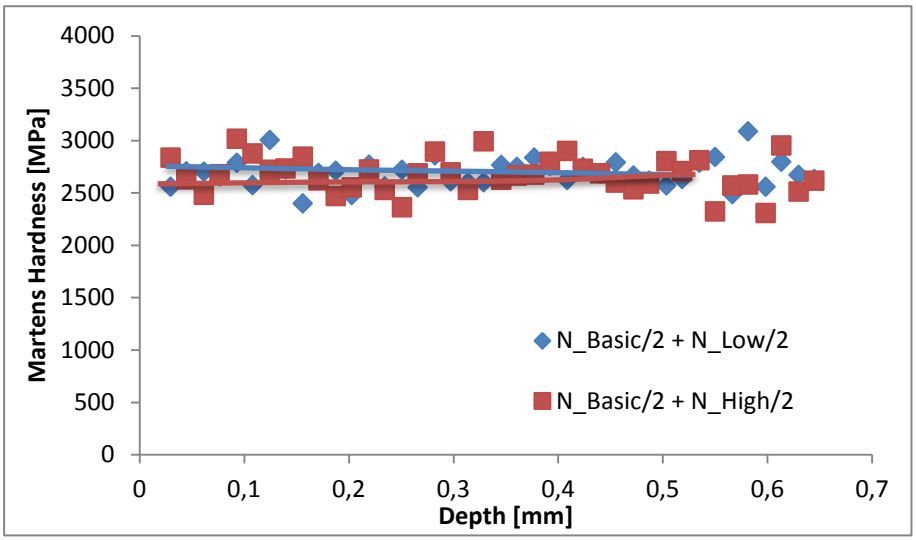

Figure 31 – Hardness depth profile for sequences N_Basic/2 N_Low/2 and N_Basic/2 +N_High/2.

To see the influence of the number of cycles of the first load amplitude applied, 100 cycles of basic load amplitude were combined with 411 086 cycles of low load amplitude and with 2303 cycles of high load amplitude. Figures 32 and 33 show the results and as can be seen, the two sequences present different compressive residual stresses at the surface. The 100_Basic + N_High/2 sequence presents lower compressive residual stress at the surface which is expected. However, a quick relaxation is observed for the 100_Basic + N_Low/2 sequence that leads to lower values of compressive residual stresses than the 100_Basic + N_High/2 sequence. A comparison between these sequences and the sequences in constant amplitude loading is shown in figures 35 and 36.

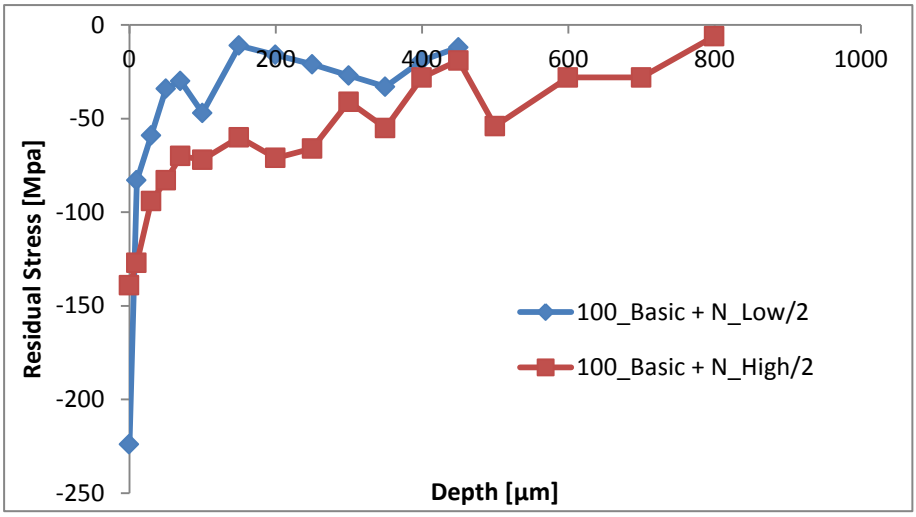

Figure 32 - Residual stress depth profile for sequences 100_Basic N_Low/2 and 100_Basic +N_High/2.

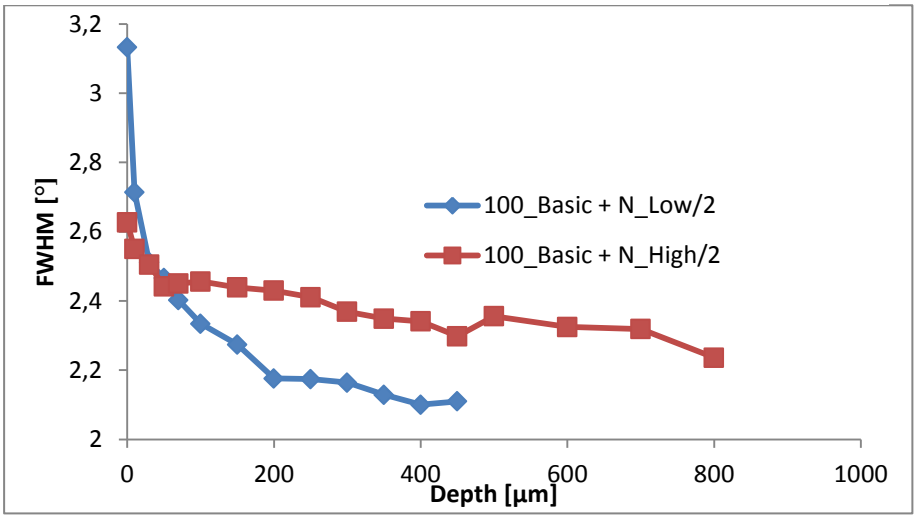

Figure 33 - FWHM depth profile for sequences 100_Basic N_Low/2 and 100_Basic +N_High/2.

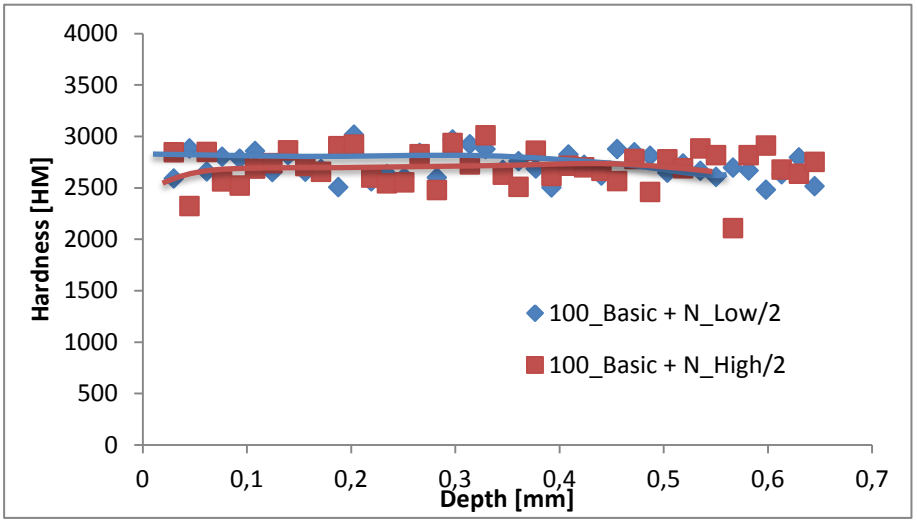

Figure 34 -Hardness depth profile for sequences 100_Basic N_Low/2 and 100_Basic +N_High/2.

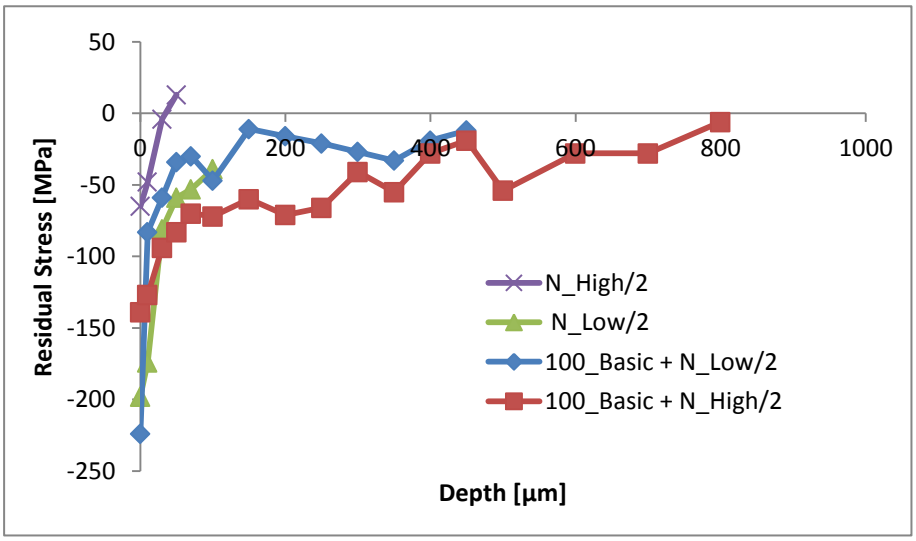

Figure 35 - Residual stress depth profile comparing constant and variable amplitude loading.

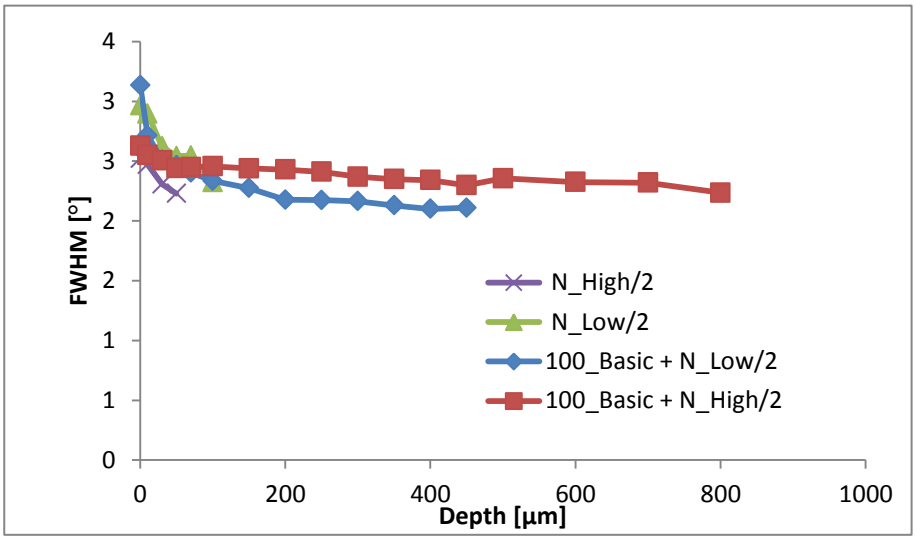

Figure 36 - FWHM depth profile comparing constant and variable amplitude loading.

In the last sequences at multi-level load done, only half of one cycle in compression or in tension with high or low load amplitude was applied after half cycles to failure of basic load amplitude. These load sequences can show the influence of the last cycle on residual stress distribution. Figure 37 depicts residual stress distribution and very distinct compressive residual stress values near the surface. Figure 39 shows hardness depth profiles for this four load sequences without trend lines.

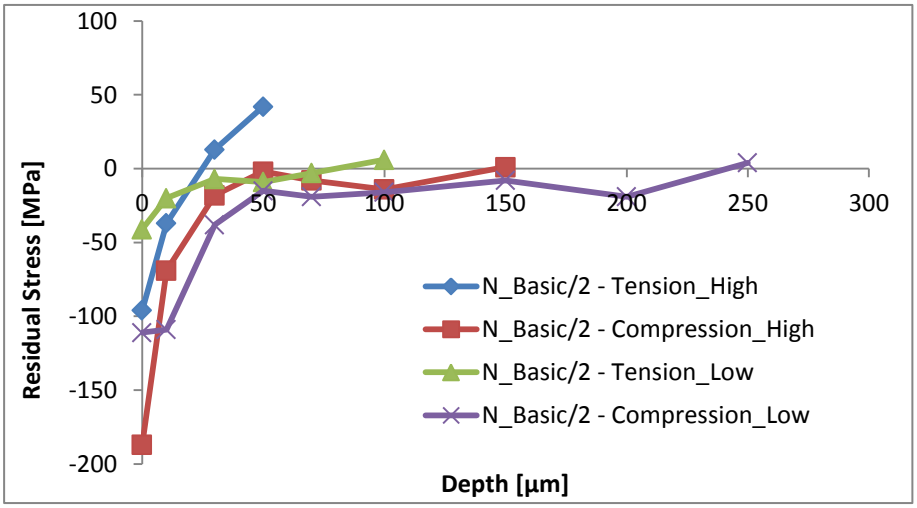

Figure 37 - Residual stress depth profile for sequences N_Basic/2 + Half Cycle.

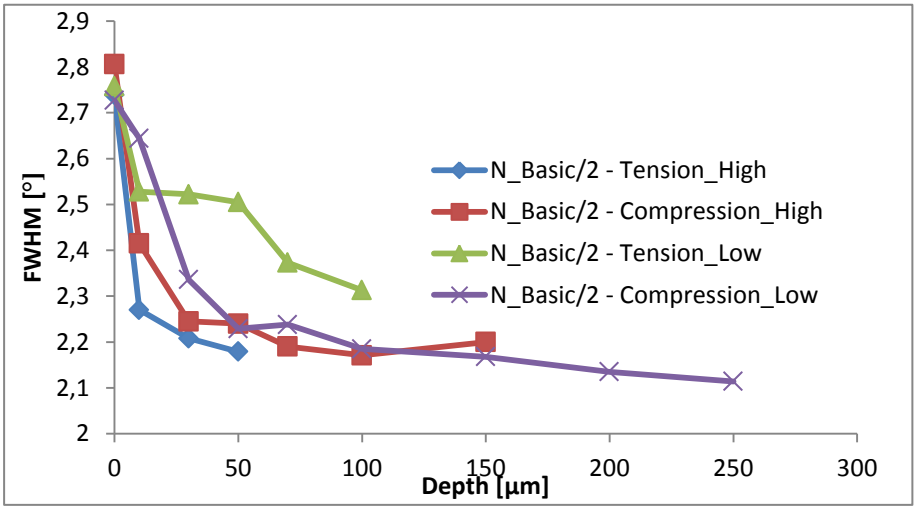

Figure 38 – FWHM depth profile for sequences N_Basic/2 + Half Cycle.

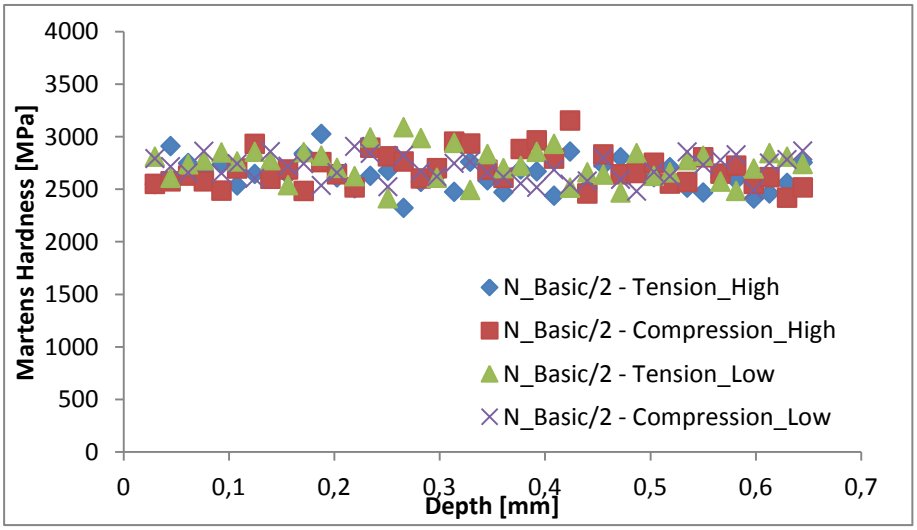

Figure 39 - Hardness depth profile for sequences N_Basic/2 + Half Cycle.

4.2. Fatigue behaviour

Fatigue behaviour is shown in cyclic deformation curves which show the plastic strain amplitude occurred in function of number of cycles. These curves are obtained by hysteresis measurements. Figure 40 shows cyclic deformation curves for different load amplitudes applied. Also is presented the cyclic deformation curve for a non-deep rolled specimen to see the effect of the mechanical surface treatment. No significant difference is observed in plastic strain amplitude between the deep rolled specimen and the non-deep rolled specimen. However, softening starts earlier for the deep rolled and is observed a little improvement of lifetime. As expected the higher the load amplitude, the higher the plastic strain amplitude occurred and the lower lifetime is observed.

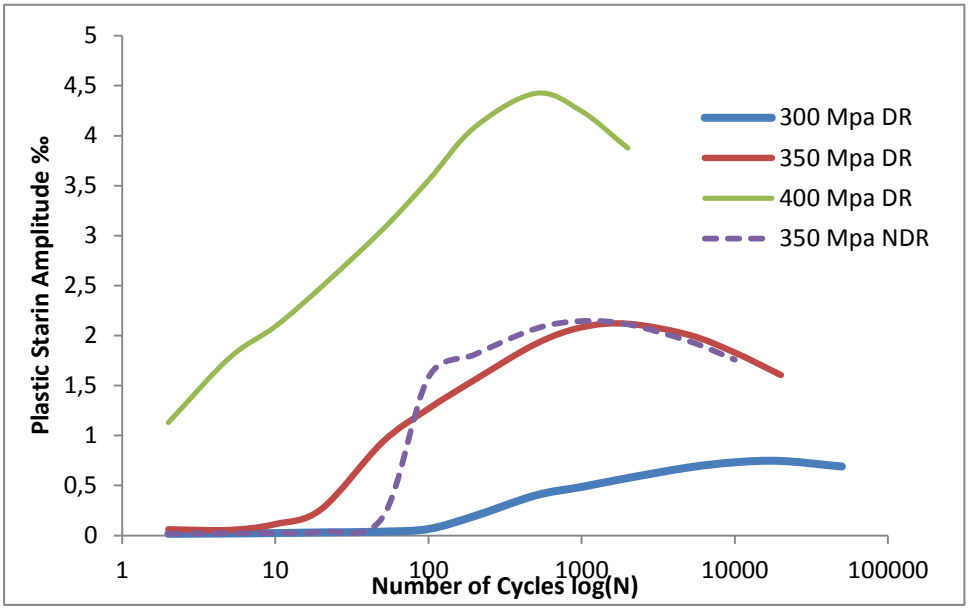

Figure 40 – Cyclic deformation behaviour for constant amplitude loading.

Fatigue behaviour for multi-level load is presented in figure 41. It is shown the cyclic deformation curves for four load sequences. It is noted a change in plastic strain amplitude when the load amplitude is changed. A decrease is observed when the low amplitude is applied that leads to longer lifetimes. The longest lifetime is detected for 100_Basic + Low combination which is expected because the specimen was subjected to less cycles of basic load. The specimen fractures quicker when the load amplitude changes after 12 500 cycles of basic load applied as can be seen in cyclic deformation curves.

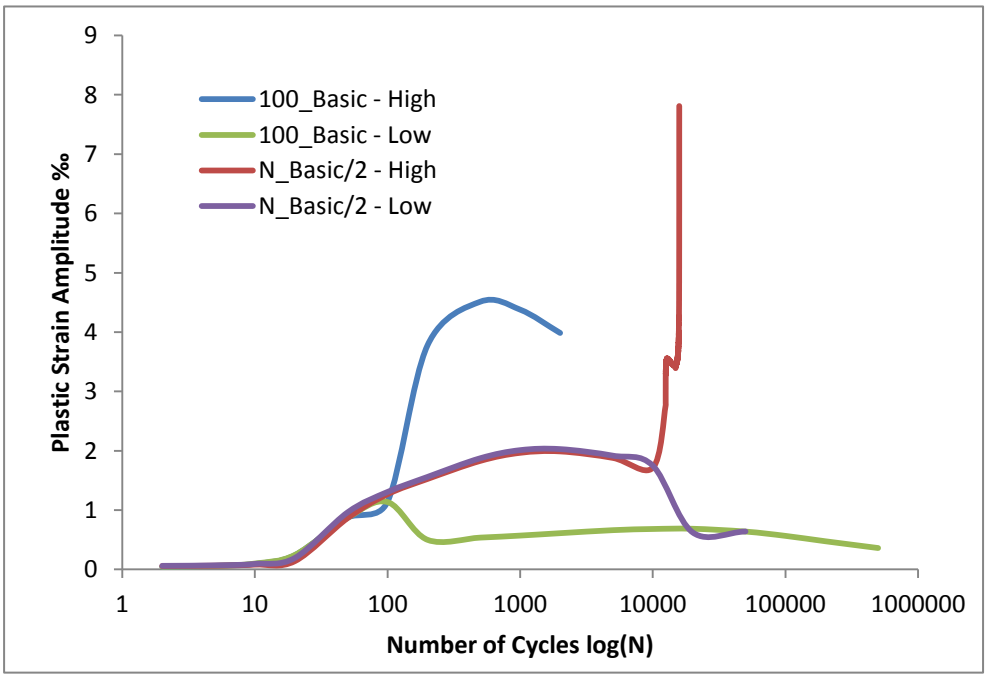

Figure 41 – Cyclic deformation curves for variable amplitude loading.

4.3. Fractography

Microscopic observations of the fractured surface were carried out in order to evaluate the portion of cross section area related to crack propagation. Fatigue crack propagation area is clearly distinct from the cracked area due to overload as can be seen in fractured area observations. Crack propagation area was calculated by software Adobe Photoshop® CS4. Figures 42, 43 and 44 show crack propagation area for all fractured specimens.

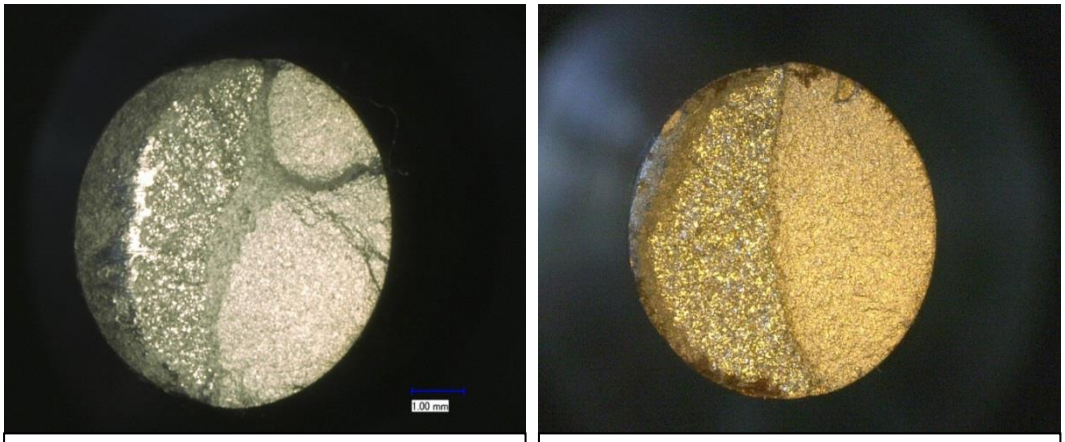

a) 11,35 mm^2 (350 MPa)

b) 12,25 mm^2 (350 MPa NDR)

Figure 42 – Fatigue crack propagation area for deep rolled and non-deep rolled specimen.

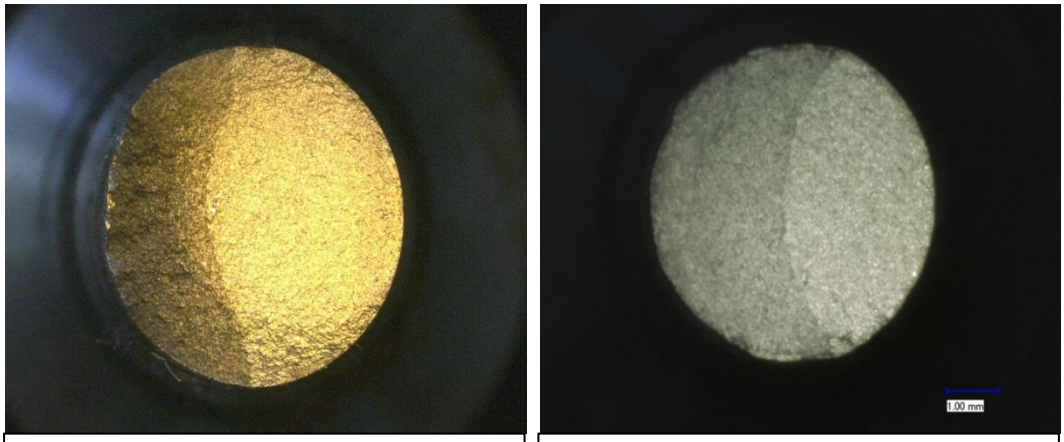

d) 15,5 mm^2 (300 MPa) | b) 11,5 mm^2 (400 MPa)

Figure 43 - Fatigue crack propagation area for low and high stress amplitude.

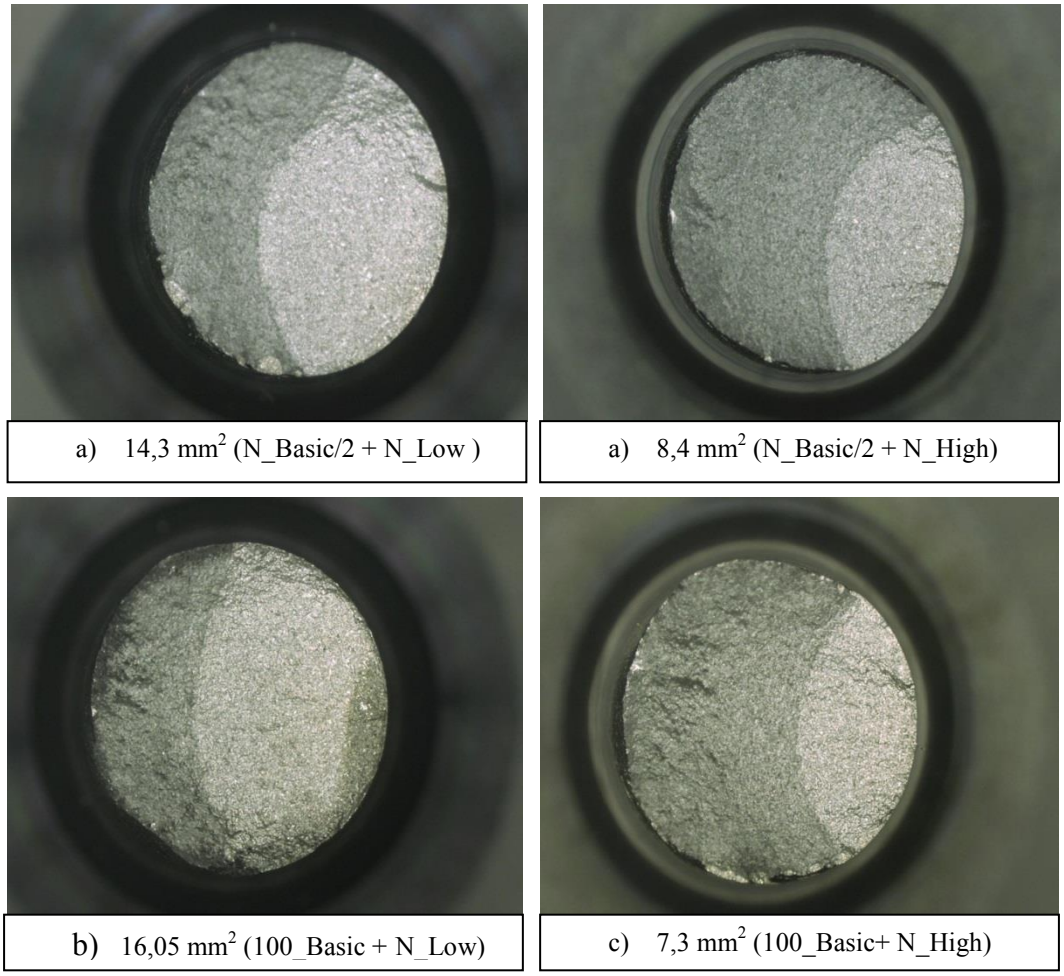

a) 14,3 mm^2 (N_Basic/2 + N_Low) | a) 8,4 mm^2 (N_Basic/2 + N_High)

b) 16,05 mm^2 (100_Basic + N_Low) | c) 7,3 mm^2 (100_Basic+ N_High)

Figure 44 - Fatigue crack propagation area at multi-level load.

5. DISCUSSION

Cyclic deformation curves shown in figure 40 are in accordance with the cyclic deformation curves obtained by Altenberger (2000) in figure 15. Lower stress amplitudes lead to lower plastic strain amplitudes and longer fatigue lifetimes. This can be linked to stability of mechanically surface treated zone in figures 23 and 24 that show more stability for lower stress amplitudes. An improvement of life is achieved for the deep rolled specimen subjected to stress amplitude of 350 MPa. Despite lifetime enhancement, no significant reduction of plastic strain amplitude is observed. This behaviour was detected and explained by Altenberger et al. (1999), for the same steel AISI 1045 subjected to low-cycle fatigue, due to non-stability of microstructure.

Near surface zone properties for non-fatigued specimen, figures 23 and 24, are expected and in accordance with the results obtained by Altenberger (2000) in figure 8. Compressive residual stress around -600 MPa were found at the surface, however, FWHM values at the surface are higher. Fatigued specimens exhibit a relaxation of initial residual stresses and FWHM values due to cyclic loading.. Residual stresses at the surface are drastically decreased and relaxation is higher for higher stress amplitudes as referred by Zhuang (2001). This behaviour was observed by Altenberger (2000) in figure 14 for the same stress amplitudes, nonetheless, with higher compressive residual stresses at the surface. Hardness depth profile in figure 31 shows similarity to FWHM distribution. Obviously, the highest hardness is obtained for non-fatigued specimen and the lowest for the fatigued specimen with the highest stress amplitude.

The load sequences with half cycles of fracture of basic amplitude plus 1000 cycles of high or low amplitude cause no significant changes in residual stress and FWHM distributions, figures 26 and 27. It appears that 1000 of cycles of high or low stress amplitude after half cycles of fracture of basic amplitude have very little influence on mechanically surface treated zone stability. However, comparing with the constant amplitude loading state, it can be observed a similar value of compressive residual stress near the surface and more stability, besides the quick relaxation in the second step of measurement.

From cyclic deformation curves in figure 41 can be seen, clearly, an increase of plastic strain amplitude when the stress amplitude changes to high amplitude. Contrarily, a decrease occurs for the low amplitude changing. Furthermore, after stress amplitude changing, the increase or decrease of plastic strain amplitude is higher after 12 500 cycles than 100 cycles of basic amplitude. Curious to observe that for both load sequences with first step of 100 cycles of basic amplitude, longer lifetimes were observed than in constant amplitude loading. For low stress amplitude in constant amplitude loading, 463 127 cycles were reached until failure, while in the load sequence after 100 cycles of basic amplitude 822 273 cycles were obtained. Lifetime improvement for sequence 100_Basic + N_High/2 is less than 200 cycles which is insignificant.

Stability of mechanically surface treated zone at multi-level load can also be seen in figures 29 and 30. They show that half lifetime to failure of high or low stress amplitude after half lifetime to failure of basic amplitude influence the stability of mechanically surface treated zone. For this case, the sequence N_Basic/2 + N_Low/2 present more stability than the N_Basic/2 + N_High/2 sequence. A change of cyclic loading to lower amplitudes than the initial leads to more stable residual stresses than the changing to high amplitude which is expected. Once more, compressive residual stress and FWHM at the surface have similar values to the state after constant amplitude loading. Interesting to note, is the different residual stresses distribution for 1000 cycles and 1662 cycles of high amplitude after the same number of cycles of basic amplitude. Compressive residual stresses are completely relaxed after 1662 cycles in figure 29, whilst they remain stable after a quick partial relaxation for 1000 cycles applied in figure 26.

As depicted in figures 32 and 33, a big difference of compressive residual stresses and FWHM near the surface is observed for the load sequences with 100 cycles of basic amplitude. Comparing with figure 29, where no significant influence is noted for the compressive residual stresses at the surface, it can be stated that the number of cycles of the first step in a load sequence influences the mechanically surface treated zone stability. Moreover, is shown a quick relaxation in the second step of measurement for the sequence 100_Basic + N_Low/2 that leads to lower compressive residual stresses than the 100_Basic + N_High/2 sequence which exhibits good stability. Also, higher values of FWHM along the depth are observed for this load sequence. This behaviour can be explained by the large number of cycles that the 100_Basic + N_Low/2 specimen was subjected (411 086 cycles

of low amplitude against 2303 cycles of high amplitude). Figures 35 and 36 show the comparison between constant amplitude loading and variable amplitude loading with the first load block of 100 cycles of basic amplitude. It can be seen that in variable amplitude loading the residual stress relaxation is lower. This behaviour is unexpected and it would be necessary more fatigue tests with different sequences and microstructure observations to understand this behaviour.

The effect of half cycle of different stress amplitude in the end of a constant amplitude loading is notorious in figure 37. It appears that the type of the load has more influence than the load amplitude. Ending in tension means lower compressive residual stresses at the surface than ending in compression independently on load amplitude. However, is observed that the sequence with the ending in low load amplitude lead to lower compressive residual stresses in both cases. It was expected that high load amplitude conduct to lower compressive residual stresses at the surface.

From fractography results, it can be seen that in constant amplitude loading higher stress amplitudes lead to smaller crack propagation areas. Oppositely, the smallest crack propagation area is observed for the lowest stress amplitude. From figure 46 it can be shown that non-deep rolled specimen has bigger crack propagation area than deep rolled specimen as a result of induced compressive residual stresses that retard crack propagation.

6. CONCLUSIONS

Cyclic deformation behaviour in constant amplitude loading for deep rolled specimens is in accordance with typical curves for this material. High plastic strain amplitudes and low fatigue lifetimes are obtained for high stress amplitudes. Different cyclic deformation behaviour is observed for non-deep rolled specimen that leads to lower fatigue lifetime than the deep rolled specimen.

The initial deep rolled state of steel AISI 1045 is characterized by a high compressive residual stress near the surface and typical residual stress, FWHM, and microhardness distribution. Fatigued specimens show residual stress relaxation due to cyclic loading. The relaxation is higher for higher stress amplitudes.

Cyclic deformation behaviour at multi-level shows an increase or decrease of plastic strain amplitude when occurs a load change to high or low amplitude, respectively. The amount of this increase or decrease of plastic strain amplitude depends on number of cycles of the previous load block in variable amplitude loading. Longer lifetimes are obtained for sequences with low amplitude than high amplitude after a load block of basic amplitude.

Near surface properties of mechanically surface treated materials in variable amplitude loading depends on number of cycles and stress amplitude of each load block in variable amplitude loading. Sequences with Basic-Low amplitude show more stability.

In variable amplitude loading, formed by a block of basic amplitude ending in half cycle of different amplitude, the type of loading has more influence on residual stress relaxation than load amplitude. Residual stress relaxation is higher when the load ends in tension than in compression independently on stress amplitude. Nonetheless, ending in high amplitude leads to higher compressive stresses than ending in low amplitude.

Fractography shows that higher stress amplitudes lead to higher crack propagation areas due to longer crack lengths caused.

REFERENCES

9th European Conference on Residual Stresses (2013), Acessed in 6th of November of 2013, in: http://ecrs9.utt.fr/index.htm

Almer, J. D., Cohen, J. B., Moran, B. (2000), "The effects of macrostreses and microstresses on fatigue crack initiation", Materials Science and Engineering, A284 (2000), 268–279.

Altenberger, I. (2000), "Mikrostrukturelle Untersuchungen mechanisch randschichtverfestigter Bereiche schwingend beanspruchter metallischer Werkstoffe", PhD Thesis, Institut für Werkstofftechnik – Metallische Werkstoffe, University of Kassel, Kassel (in German).

Altenberger, I. (2003), "Alternative mechanical surface treatments: microstructures, residual stresses and fatigue behaviour". In: Wagner, L., "Shot Peening", Wiley-VCH, Germany. pp. 421-434

Altenberger, I. (2005a), "Deep Rolling – The past, the present and the future", Proceedings of the 9th International Conference on Shot Peening, Paris, France, 2005. pp. 144-145.

Altenberger, I. (2005b), "Alternative mechanical surface treatments for fatigue strength enhancement", Materials Science Forum Vols. 490-491 (2005), pp. 328-333.

Altenberger, I., Martin, U., Scholtes, B., Oettel, H. (1999b), "Near Surface microstructures in mechanically surface treated materials and their consequences", Proceedings of the 7th International Conference on Shot Peening, Warsaw, Poland, 1999. pp. 79-87.

Altenberger, I., Nikitin, I., Scholtes, B. (2005), "Static and dynamic strain ageing of deep rolled plain carbon steel SAE 1045 for optimized fatigue strength", Proceedings of the 9th International Conference on Shot Peening, Paris, France, 2005. pp. 253-260.

Altenberger, I., Scholtes, B. (2000), "Recent developments in mechanical surface optimization", Materials Science Forum Vols. 347-349 (2000) 382-398.

Altenberger, I., Scholtes, B., Martin, U., Oettel, H. (1999a), "Cyclic deformation and near surface microstructure of shot peened or deep rolled austenitic stainless steel AISI 304" , Materials Science and Engineering A264 (1999) 1-16

Branco, C. M. (1998), "Mecânica dos Materiais", 3rd ed., Fundacao Calouste Gulbenkian, Lisboa, Portugal, (in Portuguese).

Campbell, F. C. (2008), "Elements of Metallurgy and Engineering Alloys", ASM International, U. S. A. pp 243-264.

Dalaei, K., Karlsson, B., Svensson, L. E. (2011), "Stability of shot pening induced residual stresses and their influence on fatigue lifetime", Materials Science and

Engineering, A528 (2011), 1008-1015.

Dowling, N. E. (2013), "Mechanical Behaviour of Materials – Engineering Methods for Deformation, Fracture, and Fatigue", 4th ed., Pearson, England

Eifler, D., Löhe, D., Scholtes, B. (1991), "Residual stressesand fatigue of metallic materials". In: Hauk, V., Hougardy, H., Macherauch, E., "Residual Stresses: Measurement, Calculation, Evaluation", DGM Informationgesellschaft, Germany. pp. 157-166.

Ericsson, T. (1987), "Residual stresses caused by thermal and thermomechanical surface treatments", In: Niku-Lari, A. "Advances in surface treatments: technology – applications - effects", Vol.4: Residual stresses, Pergamon Press, Great Britain. pp. 87-113.

Francois, M., Sprauel, J. M., Déhan, C. F., James, M. R., Convert, F., Lu, J., Lebrun, J. L., Hendricks, R. W. (1996), "X-ray Diffraction Method". In: Lu, J. "Handbook of Measurement of Residual Stresses, Fairmont Press, U. S. A. pp. 71-130.

Glinka, G. (1987), "Residual streses in fatigue and fracture: theoretical analyses and experiments". In: Niku-Lari, A. "Advances in surface treatments: technology – applications - effects", Vol.4: Residual stresses, Pergamon Press, Great Britain. pp. 413-454.

Hauk, V., Hougardy, H., Macherauch, E. (1991), "Residual Stresses: Measurement, Calculation, Evaluation", DGM Informationgesellschaft, Germany.

Hutchnigs, M. T., Krawitz, A. D. (1992), "Measurement o Residual and Applied Stress Using Neutron Diffraction", Kluwer Academic publishers, The Netherlands.

Juijerm, P., Altenberger, I., Scholtes, B. (2007), "Influence of ageing on cyclic deformation behaviour and residual stress relaxation of deep rolled as-quenched aluminium alloy AA6110", International Journal of Fatigue 29 (2007) 1374-1382.

Kloos, K. H., Kaiser, B., (1991), "Residual stresses induced by manufacturing". In: Hauk, V., Hougardy, H., Macherauch, E., "Residual Stresses: Measurement, Calculation, Evaluation", DGM Informationgesellschaft, Germany. pp. 205-226.

MacDougall, C., Topper, T. H. (1997), "The influence of variable amplitude loading on on crack closure and notch fatigue behaviour", International Journal Fatigue 19 (1997) 389-400.

Macherauch, E. (1987), "Introduction to Residual Stresses". In: Niku-Lari, A. "Advances in surface treatments: technology – applications - effects", Vol.4: Residual stresses, Pergamon Press, Great Britain. pp. 1-36.

Macherauch, E., Hauk, V. (1987), "Residual Stresses in Science and Technology", DGM Informationgesellschaft, Germany. Vol. 1. pp. 427-476.

Martin, U., Altenberger, I., Scholtes, B., Kremmer, K., Oettel, H. (1998), "Cyclic deformation and near surface microstructures of normalized shot peened steel SAE 1045", Material Science and Engineering A246 (1998) 69-80.

Nikitin, I., Scholtes, B., Maier, H. J., Altenberger, I. (2004), "High temperature fatigue

behaviour and residual stress stability of laser-shock peened and deep rolled austenitic steel AISI 304", Scipta Materialia 50 (2004) 1345-1350.

Niku-Lari, A. (1987), "Advances in surface treatments: technology – applications - effects", Vol.4: Residual stresses, Pergamon Press, Great Britain.

Niku-Lari, A., Lu, J., Flavenot, J. F. (1987), "Measurement of residual stresses distribution by the incremental hole-drilling method". In: Niku-Lari, A. "Advances in surface treatments: technology – applications - effects", Vol.4: Residual stresses, Pergamon Press, Great Britain. pp. 199-219.

Nobre, J. P., Kornmeier, M., Dias, A. M., Scholtes, B. (2000), "Use of the hole-drilling method for measuring residual stresses in highly stresses shot-peened surfaces", Experimental Mechanics, Vol.40 (2000), 289-297

Pommier, S. (2003); "Cyclic plasticity and variable amplitude fatigue", International Journal of Fatigue 25 (2003) 983-997

Sander M., Richard, H. A. (2006), "Fatigue crack growth under variable amplitude loading. Part I: experimental investigations". In: "Fatigue & Fracture of Enginering Materials & Structures", Vol 29, Issue 4, April 2006, Blackwell Publishing Ltd. pp. 291-301.

Schijve, J. (1976), "Observations on the prediction of fatigue crack growth propagation under variable amplitude loading". In: "Fatigue Crack Growth Under Spectrum Loads", ASTM STP 595, American Society for Testing and Materials, 1976, pp. 3-23.

Scholtes, B. (1987), "Residual stresses introduced by machining". In: Niku-Lari, A. "Advances in surface treatments: technology – applications - effects", Vol.4: Residual stresses, Pergamon Press, Great Britain. pp. 59-71.

Scientific Volume Imaging (2013), Acessed in 6th of November of 2013, in: http://www.svi.nl/Definitions

Suresh, S. (1998), "Fatigue of Materials", 2nd ed. Cambridge University Press, United Kingdom.

Vashista, M., Paul, S. (2012), "Correlation between full width at half maximum (FWHM) of XRD peak with residual stress on ground surfaces", Phylosophical Magazine, Vol. 92 (2012), 4194-4204

Wohlfahrt, H. (1987), "Residual stresses as a consequence of welding", In: Niku-Lari, A. "Advances in surface treatments: technology – applications - effects", Vol.4: Residual stresses, Pergamon Press, Great Britain. pp. 87-113.

Zhuang, W. Z., Halford, G. R. (2001), "Investigation of residual stress relaxation under cyclic load", International Journal of Fatigue 23 (2001) S.31-S37.

Zinn, W., Scholtes, B. (2002) "Residual stress formation processes during welding and joining" In: Totten, G., Howes, M., Inoue, T. "Handbook of residual stress and steel deformation", ASM International, U.S.A. pp. 391-396.